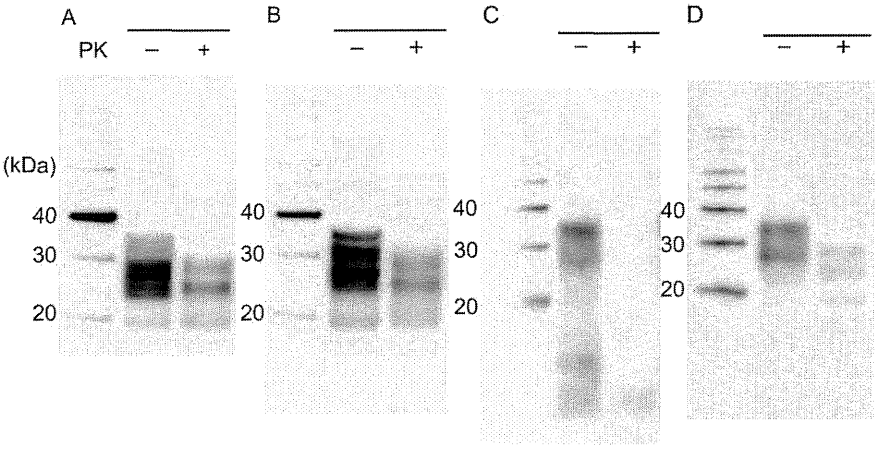

Fig. 3 Western blot analysis for PrP with or without proteinase K (PK) treatment. The brain homogenates from frontal cortices of pentosan polysulfate positive (PPS(+)) cases were separated by SDS-PAGE and probed with anti-PrP antibody (clone 3F4). The blot shows a type 1 pattern of PrP^{res} in case 1 (A) and case 2 (B). Case 3 shows PrP^{res} fragments with molecular masses of around 8 kDa (C). Case 4 shows PrP^{res} fragments with intermediate size between types 1 and 2 (D).

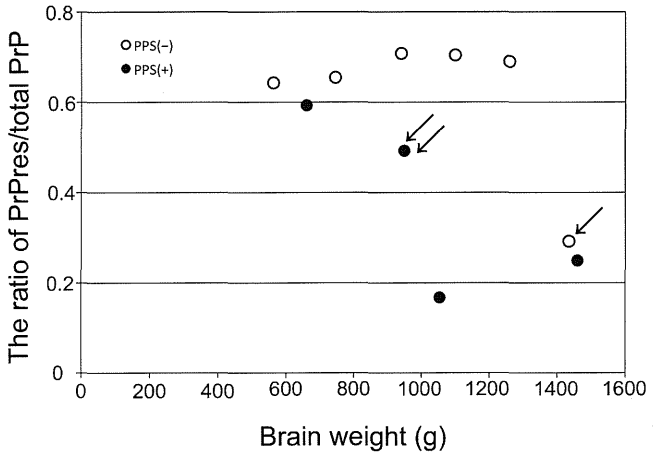

Fig. 4 Relationship between PrP^{res}/total PrP ratio and brain weight. The ratios of PrP^{res}/total PrP are markedly increased in all pentosan polysulfate negative (PPS(–)) cases (open circles) except for case 10 (arrow). Among PPS(+) cases (closed circles), case 2 (double arrows) shows a relatively low ratio of PrP^{res}/total PrP in comparison to PPS(–) cases.

atrophy. Case 2, one of three CJD cases with PPS(+), showed a relatively low ratio of PrP^{res}/total PrP in comparison to PPS(–) cases (Fig. 4).

The indices of oligomeric PrP/total PrP and monomeric PrP/total PrP

The first fraction consisted mostly of the void volume and contained insufficient protein to be assessed. Pre-column samples were taken as loading samples of total PrP. The aggregated forms of PrP were detected in fractions 2–4 (Fig. 5). Fraction 3 in this method represented the oligomeric PrP.[19,22] Thus, the index of oligomeric PrP/total PrP was obtained by dividing the intensity of fraction 3 by the intensity of the pre-column sample. Proteins with molecular weights of approximately 30 kDa, such as monomer PrP molecules, were collected mainly in fractions 6–8.[19,22] Fraction 7 represented the monomeric PrP. The index of monomeric PrP/total PrP was obtained by dividing the intensity of fraction 7 by the intensity of pre-column samples. In PPS(–) cases, the indices of oligomeric PrP/total PrP were increased according to the disease severity (Fig. 6A). Among PPS(+) cases, two CJD cases (cases 1 and 2) showed lower indices of oligomeric PrP/total PrP in comparison to PPS(–) cases. The indices of monomeric PrP/total PrP were decreased markedly in the cases with severe brain weight loss (Fig. 6B). There were no significant differences in the monomer indices between PPS(+) cases and PPS(–) cases.

DISCUSSION

Our post mortem study revealed that the PPS treatment did not apparently improve brain pathology in human prion diseases, although PPS treatment decreased the ratios of PrP^{res}/total PrP and the indices of oligomeric PrP/total PrP in some CJD cases. These findings might be relevant to apparently discrepant clinical findings: one reported no significant clinical improvements in prion diseases with PPS treatment[14,23] and the other reported that longer mean survival time in patients that had received PPS treatment was longer than previously reported for untreated specific prion diseases.[15]

The post mortem examinations revealed that neuronal loss, spongiform change and gliosis were advanced in both PPS(–) and PPS(+) cases with a greater loss of brain weight. In all PPS(+) cases, astrocytosis was evident in all layers of cerebral cortices, but GFAP expression levels were markedly reduced in the cerebral cortices, except in subpial astrocytes. CJD cases without PPS treatment usually showed strong immunoreactivity for GFAP in the cortical astrocytes as observed in case 5. Thus, we treated rat primary astrocytes with several concentrations of PPS (0 μg/mL, 0.4 μg/mL, 2.0 μg/mL, 10 μg/mL), but GFAP

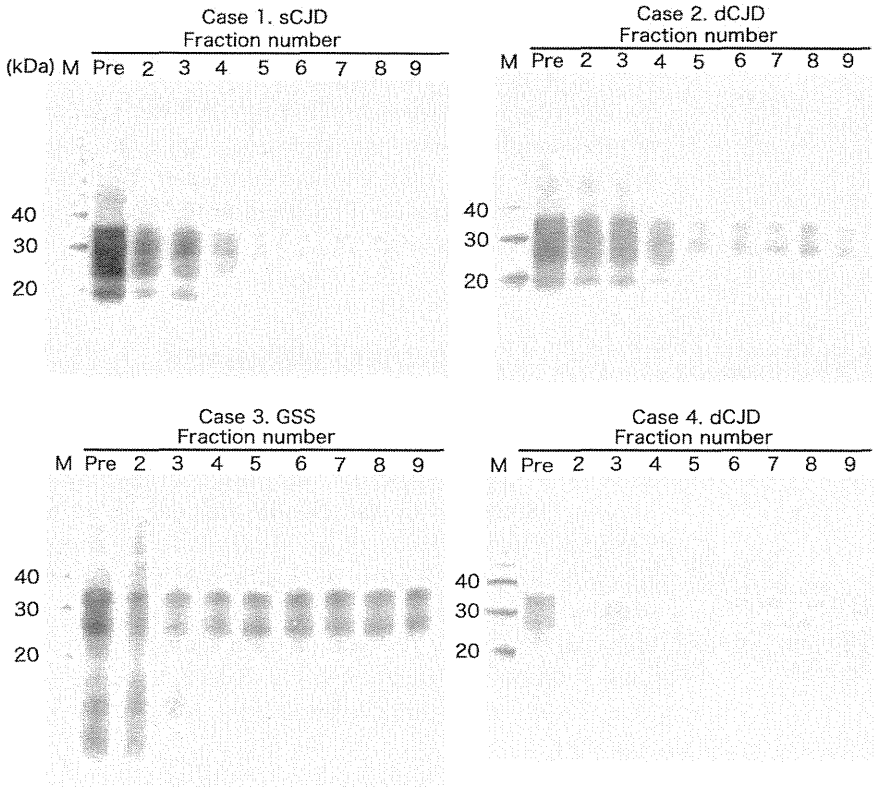

Fig. 5 Fractionation patterns of PrP in prion disease cases treated with PPS. The brain homogenate from the frontal cortex of each case was gel-filtrated without proteinase K (PK) treatment. Oligomeric PrP are detected mainly in fractions 2–4. Monomeric PrP are detected mainly in fractions 6–8. Pre: Pre-column brain homogenate.

expression levels were not significantly altered (data not shown). Therefore, we suggest that decreased GFAP expression levels in cortical astrocytes in PPS(+) cases is not due to the direct action of PPS on astrocytes.

PPS(+) cases in our study included only one case of sCJD (case 1). Although PPS infusion was started 3 months after disease onset, case 1 did not show any improvement in clinical features and the ratio of PrP^{res}/total PrP was comparable with PPS(−) sCJD cases. Meanwhile, two PPS(+) cases (cases 2 and 3) showed a relatively low ratio of PrP^{res}/total PrP. Because case 2 (dCJD) showed synaptic-type PrP deposition and type 1 PrP^{res} accumulation, it was considered to be a referential case to compare with PPS(−) CJD cases. Terada *et al.* also reported a reduction of PrP^{res} in a sCJD brain with PPS treatment.[23] In case 3 with GSS, PrP^{res} signals were very faint. It is possible that the molecular weights of plaque-type PrP deposition were too large to be detected through electrophoresis in these gels. Parchi *et al.* reported that immunoblot analysis of GSS P102L patients showed two major PrP^{res} signals with molecular masses of 21 and 8 kDa, and that the GSS patients with only the 8 kDa fragment showed mainly plaque-type PrP deposition.[24] In our study, the GSS patient with a P102L mutation showed both plaque-type PrP deposition and synaptic deposition, although Western blotting with PK treatment showed only PrP^{res} around 8 kDa. In this case, PrP^{res} might have a low resistance to PK treatment. Therefore, it may not be appropriate to compare the ratio of PrP^{res}/total PrP of case 3 to those of PPS(−) CJD cases. In case 4 with dCJD with plaque-type PrP deposits, Western blot analysis detected PrP^{res} fragments with intermediate size between types 1 and 2. Kobayashi *et al.* reported that the intermediate type PrP^{res} was seen in all examined dCJD cases with 129 methionine/methionine and plaque-type PrP deposits.[25]

Among PPS(+) cases, cases 1 and 2 showed lower indices of oligomeric PrP/total PrP than the indices of PPS(−) cases. PPS treatment might have reduced oligomeric PrP by reducing PrP^{res}. Alternatively, another study has reported that PrP fragments form amyloid aggregates in the presence of heparin which has a similar effect to PPS.[26] Therefore, oligomeric PrP in PPS(+) may be accumulated into fibrils. In our study, we did not evaluate fibrils because fibrils are difficult to electrophorese. Contrary to the reduction of oligomeric PrP/total PrP indices, monomeric PrP/total PrP indices in PPS(+) cases showed similar values to PPS(−) cases. The indices of monomeric PrP/total PrP were decreased, especially in cases with a brain weight of less than 1000 g. In these cases, PrP^{c} may have been depleted because of severe neuronal loss. Recently, oligomeric PrP was reported as the most infectious unit[17] and another study suggested that oligomeric PrP specifically inhibits the 26S proteasome, thus mediating a mechanism for intracellular neurotoxicity.[18]

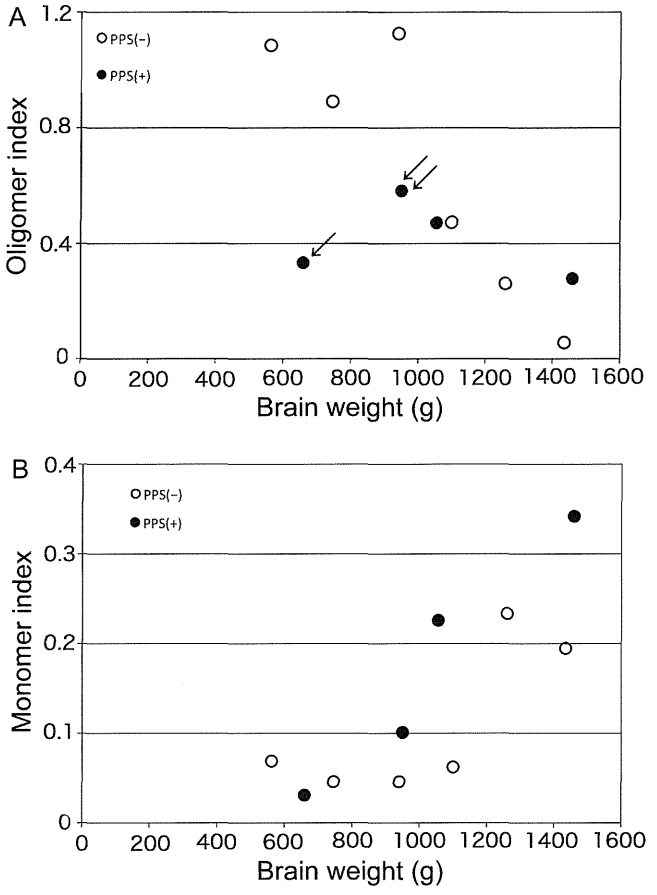

Fig. 6 Relationship between oligomeric PrP/total PrP indices and brain weight (A), or between monomeric PrP/total PrP indices and brain weight (B). (A) The oligomeric PrP/total PrP index was calculated by comparing the signals of fraction 3 to the signals of pre-column samples. In pentosan polysulfate negative (PPS(−)) cases (open circles), the oligomeric/total PrP indices are increased in accordance with brain weight loss. This tendency is also found in the PPS(+) cases (closed circles). The oligomeric PrP/total PrP indices in the PPS(+) cases are relatively low, particularly in the advanced cases with severe brain atrophy (case 1 (arrow) and case 2 (double arrows)). (B) The monomeric PrP/total PrP indices were calculated by comparing the signals of fraction 7 to the signals of pre-column samples. Monomeric PrP/total PrP indices of the advanced cases with severe brain atrophy are decreased irrespective of PPS treatment.

Doh-ura *et al.* reported that PPS infusion not only decreased PrP deposition but also reduced neurodegenerative changes in a rodent model.[9] However, in the rodent model PPS treatment could be started at the preclinical stage, whereas PPS treatment for patients was usually started at an advanced clinical stage. In the animal model, PPS treatment at an early or a late preclinical stage of the infection prolonged the incubation time by 2.4 or 1.7 times that of the control mice. Furthermore, the dosage of PPS in the animal model (460 μg/kg/day) was higher than the dosage for the human cases (120 μg/kg/day at a maximum).[9] Thus, if we could start PPS treatment at an earlier clinical stage or administer prophylactic PPS, the treatment might have beneficial effects on patients with prion diseases as shown in the experimental animal model.[9] Indeed the low indices of oligomeric PrP/total PrP were detected in two cases, but these cases showed no apparent clinicopathological improvements. Therefore, the therapeutic effects of intraventricular PPS infusion for human prion diseases are still uncertain.

ACKNOWLEDGMENTS

This work was funded by Grants-in-Aid for Scientific Research (B) (No. 22300116) and (C) (No. 21500337) from the Japan Society for the Promotion of Science (JSPS) and by the Health and Labor Sciences Research Grants (Research on Measures for Intractable Diseases) from the Ministry of Health, Labor and Welfare of Japan. The authors thank Ms Sachiko Koyama for her technical assistance. The authors also thank Drs Yoshio Tsuboi, Nobutaka Ishizu, Hiroshi Kurisaki and Shigeo Murayama for providing clinical data and pathological materials.

REFERENCES

1. Creutzfeldt HG. On a particular focal disease of the central nervous system (preliminary communication), 1920. *Alzheimer Dis Assoc Disord* 1989; **3**: 3–25.
2. Prusiner SB. Prions. *Proc Natl Acad Sci USA* 1998; **95**: 13363–13383.
3. Doh-Ura K, Iwaki T, Caughey B. Lysosomotropic agents and cysteine protease inhibitors inhibit scrapie-associated prion protein accumulation. *J Virol* 2000; **74**: 4894–4897.
4. Korth C, May BC, Cohen FE, Prusiner SB. Acridine and phenothiazine derivatives as pharmacotherapeutics for prion disease. *Proc Natl Acad Sci USA* 2001; **98**: 9836–9841.
5. Barret A, Tagliavini F, Forloni G *et al.* Evaluation of quinacrine treatment for prion diseases. *J Virol* 2003; **77**: 8462–8469.
6. Collins SJ, Lewis V, Brazier M, Hill AF, Fletcher A, Masters CL. Quinacrine does not prolong survival in a murine Creutzfeldt-Jakob disease model. *Ann Neurol* 2002; **52**: 503–506.
7. Collinge J, Gorham M, Hudson F *et al.* Safety and efficacy of quinacrine in human prion disease (PRION-1 study): a patient-preference trial. *Lancet Neurol* 2009; **8**: 334–344.
8. Caughey B, Brown K, Raymond GJ, Katzenstein GE, Thresher W. Binding of the protease-sensitive form of

PrP (prion protein) to sulfated glycosaminoglycan and congo red [corrected]. *J Virol* 1994; **68**: 2135–2141.
9. Doh-ura K, Ishikawa K, Murakami-Kubo I *et al.* Treatment of transmissible spongiform encephalopathy by intraventricular drug infusion in animal models. *J Virol* 2004; **78**: 4999–5006.
10. Caughey B, Raymond GJ. Sulfated polyanion inhibition of scrapie-associated PrP accumulation in cultured cells. *J Virol* 1993; **67**: 643–650.
11. Shyng SL, Lehmann S, Moulder KL, Harris DA. Sulfated glycans stimulate endocytosis of the cellular isoform of the prion protein, PrPC, in cultured cells. *J Biol Chem* 1995; **270**: 30221–30229.
12. Todd NV, Morrow J, Doh-ura K *et al.* Cerebroventricular infusion of pentosan polysulphate in human variant Creutzfeldt-Jakob disease. *J Infect* 2005; **50**: 394–396.
13. Rainov NG, Tsuboi Y, Krolak-Salmon P, Vighetto A, Doh-Ura K. Experimental treatments for human transmissible spongiform encephalopathies: is there a role for pentosan polysulfate? *Expert Opin Biol Ther* 2007; **7**: 713–726.
14. Tsuboi Y, Doh-Ura K, Yamada T. Continuous intraventricular infusion of pentosan polysulfate: clinical trial against prion diseases. *Neuropathology* 2009; **29**: 632–636.
15. Bone I, Belton L, Walker AS, Darbyshire J. Intraventricular pentosan polysulphate in human prion diseases: an observational study in the UK. *Eur J Neurol* 2008; **15**: 458–464.
16. Caughey B, Lansbury PT. Protofibrils, pores, fibrils, and neurodegeneration: separating the responsible protein aggregates from the innocent bystanders. *Annu Rev Neurosci* 2003; **26**: 267–298.
17. Silveira JR, Raymond GJ, Hughson AG *et al.* The most infectious prion protein particles. *Nature* 2005; **437**: 257–261.
18. Kristiansen M, Deriziotis P, Dimcheff DE *et al.* Disease-associated prion protein oligomers inhibit the 26S proteasome. *Mol Cell* 2007; **26**: 175–188.
19. Minaki H, Sasaki K, Honda H, Iwaki T. Prion protein oligomers in Creutzfeldt-Jakob disease detected by gel-filtration centrifuge columns. *Neuropathology* 2009; **29**: 536–542.
20. Lue LF, Kuo YM, Roher AE *et al.* Soluble amyloid beta peptide concentration as a predictor of synaptic change in Alzheimer's disease. *Am J Pathol* 1999; **155**: 853–862.
21. Sharon R, Bar-Joseph I, Frosch MP, Walsh DM, Hamilton JA, Selkoe DJ. The formation of highly soluble oligomers of alpha-synuclein is regulated by fatty acids and enhanced in Parkinson's disease. *Neuron* 2003; **37**: 583–595.
22. Sasaki K, Minaki H, Iwaki T. Development of oligomeric prion-protein aggregates in a mouse model of prion disease. *J Pathol* 2009; **219**: 123–130.
23. Terada T, Tsuboi Y, Obi T *et al.* Less protease-resistant PrP in a patient with sporadic CJD treated with intraventricular pentosan polysulphate. *Acta Neurol Scand* 2010; **121**: 127–130.
24. Parchi P, Chen SG, Brown P *et al.* Different patterns of truncated prion protein fragments correlate with distinct phenotypes in P102L Gerstmann-Straussler-Scheinker disease. *Proc Natl Acad Sci USA* 1998; **95**: 8322–8327.
25. Kobayashi A, Asano M, Mohri S, Kitamoto T. Cross-sequence transmission of sporadic Creutzfeldt-Jakob disease creates a new prion strain. *J Biol Chem* 2007; **282**: 30022–30028.
26. Cortijo-Arellano M, Ponce J, Durany N, Cladera J. Amyloidogenic properties of the prion protein fragment PrP(185-208): comparison with Alzheimer's peptide Abeta(1-28), influence of heparin and cell toxicity. *Biochem Biophys Res Commun* 2008; **368**: 238–242.

Clinical/Scientific Notes

M. Omoto, MD
S. Suzuki, MD
T. Ikeuchi, MD
T. Ishihara, MD
T. Kobayashi, MD
Y. Tsuboi, MD
J. Ogasawara, MD
M. Koga, MD
M. Kawai, MD
T. Iwaki, MD
T. Kanda, MD

AUTOSOMAL DOMINANT TAUOPATHY WITH PARKINSONISM AND CENTRAL HYPOVENTILATION

Frontotemporal dementia and parkinsonism linked to chromosome 17 (FTDP-17T) can show various clinical phenotypes.[1] We describe Japanese siblings with the intronic 10 + 14 splice site mutation of the microtubule-associated protein tau (MAPT) gene, showing parkinsonism, depression, weight loss, and central hypoventilation with reduced serotonin concentration suggested by low 5-hydroxyindole acetic acid (5-HIAA) in CSF. These clinical and biochemical features are just shared by Perry syndrome,[2-4] although neither *DCTN1* gene mutation nor TDP-43 proteinopathy was found.

Case reports. A Japanese woman (III-5) (figure, A) developed clumsiness, tremor of the upper limbs, appetite loss, and apathy at age 44. She had lost 14 kilograms of body weight during 10 months. Mask-like face, hypophonic voice, bradykinesia, and muscle rigidity with predominance on the right side were observed. Deep tendon reflexes were hyperactive, especially in the right extremities with the Babinski sign. Despite levodopa treatment, her parkinsonism progressed and memory loss, disorientation, and cyanosis became apparent. Blood tests, EKG, and chest X-ray were not remarkable. Arterial blood gases showed reduced oxygen (60.3 Torr) and increased carbon dioxide (55.5 Torr). CSF analysis showed reduced 5-HIAA (5.6 ng/mL [normal 28.5 ± 7.2 ng/mL]). Brain MRI demonstrated mild atrophy in the brainstem tegmentum. Polysomnography revealed central hypoventilation with hypoxia. Although memory loss, disorientation, and apathy improved under ventilation assistance, she died due to sudden apnea, 22 months after the onset. Autopsy examination showed severe neuronal loss with gliosis in the globus pallidus, dentate nucleus, subthalamic nucleus, substantia nigra, locus ceruleus, and brainstem tegmentum including the dorsal raphe. Phosphorylated-tau-positive globose-type neurofibrillary tangles, neuropil threads, and oligodendroglial inclusions were seen in the above lesions. These structures were positive for 4 repeat (4R) tau, but negative for TDP-43. In addition to these typical progressive supranuclear palsy (PSP) pathologies, she also showed severe gliosis, rarefaction, and 4R tau deposition in widespread areas of ventrolateral medulla oblongata including the pre-Bötzinger complex (figure, B–M). Sequencing of all coding exons of tau gene revealed a heterozygous C-to-T substitution at + 14th downstream of exon 10. Immunoblot analysis of dephosphorylated samples using phosphorylation-independent anti-tau antibody revealed 2 major bands that aligned with the recombinant 4R tau isoforms, equivalent to PSP and corticobasal degeneration cases (figure, N). Further, by immunoblot using sarkosyl-insoluble brain extracts, a tau fragment of 33 kDa similar to PSP was observed (figure, O). These findings suggest that she shares both histopathologic and biochemical features of tauopathy with PSP.

The younger sister of the proband (III-6) presented with delusion and hallucination at age 19. Neurologic examination at age 43 showed slight spasticity of lower limbs. Like her sister, CSF analysis revealed reduced 5-HIAA (13.8 ng/mL), and the same *MAPT* gene mutation was detected. The proband's mother (II-8) showed parkinsonism at age 48, and despite levodopa treatment, became bedridden and almost mute 1 year later, and died at age 54.

Discussion. An English consanguineous kindred with central hypoventilation and parkinsonism was reported to have the *MAPT* gene mutation, in which extensive tauopathy in the tegmental medullary neurons and a novel homozygous S352L mutation in exon 12 of the *MAPT* gene were found.[5] In comparison with this family, in which occasional tau deposition in medullary white matter was seen, the proband showed severer tau deposition in the widespread areas of ventrolateral medulla oblongata. This family showed a recessive mode of inheritance and further details of the neuropathology and serotonin/5-HIAA concentration in the CSF were not available.

In addition to PSP pathology, the proband also showed severe degeneration in widespread areas including the dorsal raphe, an area containing serotonergic neurons and known to be chemosensitive to hypercapnia, and the ventrolateral medulla including the pre-Bötzinger complex, a part of the ventral respiratory group shown to be critical for generation of the normal respiratory rhythm.[6] These pathologic changes as well as

Figure Family pedigree, histopathologic findings, and immunoblot analyses

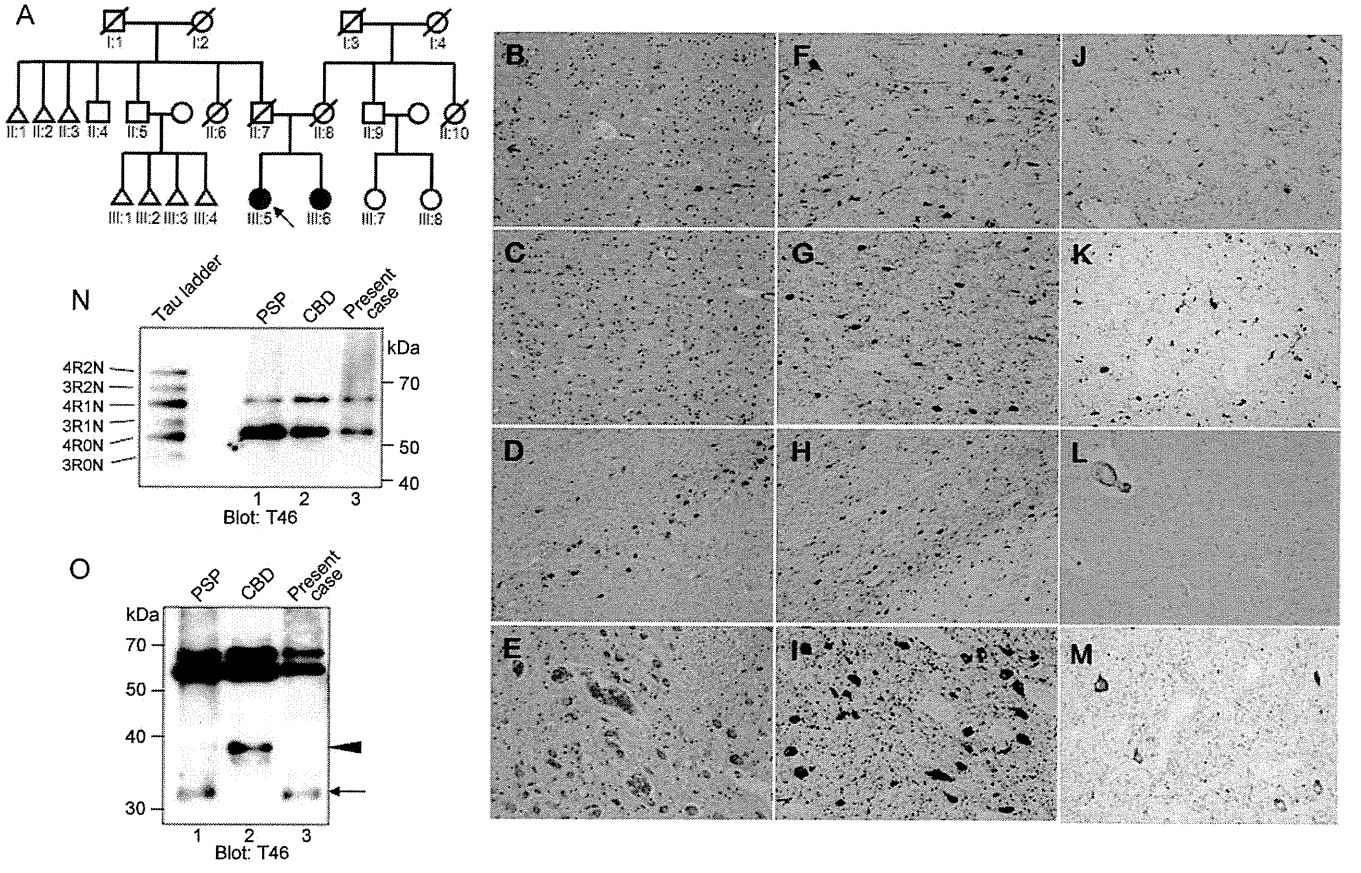

(A) The family pedigree. The proband is III-5 (arrow). She and her younger sister are found with the intronic 10 + 14 splice site mutation of the *MAPT* gene. Histopathologic findings: (B–E) hematoxylin-eosin staining, (F–I, M) immunohistochemistry with anti-phosphorylated tau antibody AT8, (J) anti-GFAP antibody, (K) anti-4 repeat tau RD4 antibody, and (L) anti-phosphorylated-TDP-43 antibody. (B, F, J–L) Globus pallidus. (C, G) Subthalamic nucleus. (D, H) Substantia nigra. (E, I) Locus ceruleus. (M) Ventrolateral medulla. (B–E, J) Severe neuronal loss with gliosis is noted in the globus pallidus, subthalamic nucleus, substantia nigra, and locus ceruleus. (F–I, M) Phosphorylated tau-positive globose-type neurofibrillary tangles, neuropil threads, and oligodendroglial inclusions are seen in the above lesions. (K) Shown are dense depositions of 4-repeat tau. (L) All section of the cerebrum, brainstem, cerebellum, and spinal cord are TDP-43 negative. (M) Ventrolateral medulla also shows dense deposition of phosphorylated tau-immunopositive structures. Original magnification ×200 (E, I, M); ×100 (B–D, F–H, J–L). Immunoblot analysis: (N) immunoblot analysis of the sarkosyl-insoluble fraction after dephosphorylation extracted from the brains of progressive supranuclear palsy (PSP) (lane 1), corticobasal degeneration (CBD) (lane 2), and the proband (lane 3). Six recombinant human tau isoforms are indicated on the left (Tau ladder). Sarkosyl-insoluble tau in the proband consists predominantly of 4R tau isoforms (4R0N and 4R1N), similar to those in PSP and CBD cases. (O) Immunoblot analysis of the sarkosyl-insoluble fraction before dephosphorylation. The pattern of low-molecular-mass tau fragments in a PSP case shows a prominent band of 33 kDa (lane 1, arrow), while that in a CBD case shows a prominent band of 37 kDa (lane 2, arrowhead). The proband (lane 3) exhibited 33 kDa of tau fragment, similar to the PSP case.

reduction in CSF serotonin metabolite suggest that central hypoventilation might have been caused by mechanisms similar to those of Perry syndrome.[7] Clinical and laboratory features of Perry syndrome, parkinsonism, depression, weight loss, and central hypoventilation with reduced 5-HIAA concentration in CSF, are also caused by mutations of *MAPT*, especially the intronic 10 + 14 mutation, which develops 4R tauopathy.

From the Department of Neurology and Clinical Neuroscience (M.O., J.O., M. Koga, M. Kawai, T. Kanda), Yamaguchi University Graduate School of Medicine, Yamaguchi; Department of Neuropathology (S.S., T. Iwaki), Neurological Institute, Kyushu University Graduate School of Medical Science, Fukuoka; Department of Molecular Neuroscience (T. Ikeuchi, T. Ishihara), Brain Research Institute, Niigata University, Niigata; and Department of Neurology (T. Kobayashi, Y.T.), Fukuoka University School of Medicine, Fukuoka, Japan.

Author contributions: Study concept and design: Drs. Omoto and Kanda; acquisition of data: Drs. Omoto, Suzuki, Kobayashi, Ikeuchi, Ishihara, and Kanda; analysis and interpretation: Drs. Omoto, Suzuki, Koga, and Kanda; drafting of the manuscript: Drs. Omoto, Koga, and Kanda; critical revision of the manuscript for important intellectual content: Drs. Suzuki, Ikeuchi, Tsuboi, Ogasawara, Kawai, and Iwaki; study supervision: Drs. Tsuboi, Iwaki, and Kanda; all the authors have seen and approved the final version of the manuscript.

Disclosure: The authors report no disclosures.

Correspondence & reprint requests to Dr. Kanda: tkanda@yamaguchi-u.ac.jp

Received June 11, 2011. Accepted in final form November 4, 2011.

1. Ghetti B, Hutton ML, Wszolek ZK. Frontotemporal dementia and parkinsonism linked to chromosome 17 associ-

ated with tau gene mutations (FTDP-17T). In: Dickson DW, ed. Neurodegeneration: The Molecular Pathology of Dementia and Movement Disorders. Basel: Neuropathologica Press; 2003:86–102.
2. Perry TL, Bratty PJ, Hansen S, Kennedy J, Urquhart N, Dolman CL. Hereditary mental depression and parkinsonism with taurine deficiency. Arch Neurol 1975;32:108–113.
3. Farrer MJ, Hulihan MM, Kachergus JM. DCTN1 mutations in Perry syndrome. Nature Genet 2009;41:163–165.
4. Wider C, Dickson DW, Stoessl AJ, et al. Pallidonigral TDP-43 pathology in Perry syndrome. Parkinsonism Relat Disord 2009;15:281–286.
5. Nicholl DJ, Greenstone MA, Clarke CE, et al. An English kindred with a novel recessive tauopathy and respiratory failure. Ann Neurol 2003;54:682–686.
6. Bolton CF, Chen R, Wijdicks EFM, Zifko U. Anatomy and physiology of the nervous system control of respiration. In: Bolton C, Chen R, Wijdicks EFM, et al., eds. Neurology of Breathing. Philadelphia: Butterworth- Heinemann; 2004:19–35.
7. Tsuboi Y, Dickson DW, Nabeshima K, et al. Neurodegeneration involving putative respiratory neurons in Perry syndrome. Acta Neuropathol 2008;115:263–268.

Editor's Note to Authors and Readers: Levels of Evidence coming to *Neurology*®

Effective January 15, 2009, authors submitting Articles or Clinical/Scientific Notes to *Neurology*® that report on clinical therapeutic studies must state the study type, the primary research question(s), and the classification of level of evidence assigned to each question based on the classification scheme requirements shown below (left). While the authors will initially assign a level of evidence, the final level will be adjudicated by an independent team prior to publication. Ultimately, these levels can be translated into classes of recommendations for clinical care, as shown below (right). For more information, please access the articles and the editorial on the use of classification of levels of evidence published in *Neurology*.[1-3]

REFERENCES

1. French J, Gronseth G. Lost in a jungle of evidence: we need a compass. Neurology 2008;71:1634–1638.
2. Gronseth G, French J. Practice parameters and technology assessments: what they are, what they are not, and why you should care. Neurology 2008;71:1639–1643.
3. Gross RA, Johnston KC. Levels of evidence: taking *Neurology*® to the next level. Neurology 2009;72:8–10.

Classification scheme requirements for therapeutic questions

Class I. A randomized, controlled clinical trial of the intervention of interest with masked or objective outcome assessment, in a representative population. Relevant baseline characteristics are presented and substantially equivalent among treatment groups or there is appropriate statistical adjustment for differences.

Class II. A randomized, controlled clinical trial of the intervention of interest in a representative population with masked or objective outcome assessment that lacks one criterion a-e in Class I or a prospective matched cohort study with masked or objective outcome assessment in a representative population that meets b-e in Class I. Relevant baseline characteristics are presented and substantially equivalent among treatment groups or there is appropriate statistical adjustment for differences.

Class III. All other controlled trials (including well-defined natural history controls or patients serving as their own controls) in a representative population, where outcome is independently assessed, or independently derived by objective outcome measurements.

Class IV. Studies not meeting Class I, II, or III criteria including consensus or expert opinion.

AAN classification of recommendations

A = Established as effective, ineffective, or harmful (or established as useful/predictive or not useful/predictive) for the given condition in the specified population. (Level A rating requires at least two consistent Class I studies.)

B = Probably effective, ineffective, or harmful (or probably useful/predictive or not useful/predictive) for the given condition in the specified population. (Level B rating requires at least one Class I study or two consistent Class II studies.)

C = Possibly effective, ineffective, or harmful (or possibly useful/predictive or not useful/predictive) for the given condition in the specified population. (Level C rating requires at least one Class II study or two consistent Class III studies.)

U = Data inadequate or conflicting; given current knowledge, treatment (test, predictor) is unproven.

NEUROPATHOLOGY

Neuropathology 2012; **32**, 69–76 doi:10.1111/j.1440-1789.2011.01222.x

Case Report

Extensive distribution of glial cytoplasmic inclusions in an autopsied case of multiple system atrophy with a prolonged 18-year clinical course

Kenta Masui,[1] Yukako Nakata,[2] Naoki Fujii[2] and Toru Iwaki[1]

[1]Department of Neuropathology, Neurological Institute, Graduate School of Medical Sciences, Kyushu University and [2]Department of Neurology, Neuro-Muscular Center, National Omuta Hospital, Fukuoka, Japan

We describe herein an autopsied case of multiple system atrophy (MSA) with prolonged clinical course of 18 years, and evaluate the extent of neurodegeneration and glial cytoplasmic inclusions (GCIs) in the entire brain of this rare case. A 64-year-old woman presented with typical neurological symptoms and imaging features of MSA. Thereafter, she became bedridden, and breathing was assisted through a tracheostomy for 12 years. She died at the age of 82 after 18 years from the initial symptom. Post mortem examination revealed severe neurodegeneration in the inferior olive, pontine nuclei, substantia nigra, locus ceruleus, putamen and cerebellum. Notably, phosphorylated α-synuclein (p-α-syn)-positive GCIs were found in these areas, but their number was very low. In contrast, the density of GCIs was much higher in such regions as the tectum/tegmentum of the brainstem, pyramidal tracts, neocortices and limbic system, which usually contain a small number of GCIs. Another constituent of GCIs, ubiquitin (Ub) and Ub-associated autophagy substrate p62, were also positive in some GCIs, and distribution of Ub/p62 immunoreactivity was proportionate to that of p-α-syn+ GCIs despite the very long duration of the disease. Furthermore, this case had complicated hypoxic encephalopathy, but p-α-syn+ GCIs were also found in the damaged white matter, indicating the contribution of α-syncleinopathy as well as hypoxic effect to the secondary myelin and axonal loss in the white matter. Together, this rare case suggests the contribution of the disease duration to the prevalence of GCIs, and the possible involvement of the limbic system in extensive-stage disease.

Key words: glial cytoplasmic inclusion, multiple system atrophy, prolonged clinical course, ubiquitin, α-synuclein.

INTRODUCTION

Multiple system atrophy (MSA) is a nonhereditary, late-onset progressive neurodegenerative disorder which exhibits autonomic dysfunction, poorly levodopa-responsive parkinsonism or cerebellar ataxia.[1] Originally, MSA was described as three apparently separate entities,[2] and subdivided into olivopontocerebellar atrophy (OPCA), striatonigral degeneration (SND) and Shy-Drager syndrome (SDS). Pathological confirmation of MSA came with the description of glial cytoplasmic inclusions (GCIs)[3,4] which were later found to be α-synuclein-positive,[5–7] leading to the recognition that MSA is a glial α-synucleinopathy.[8]

The natural course of MSA is progressive and highly disabling, and mean survival ranges between 7 and 9 years after first clinical presentation, although there may be substantial variation.[9] Several studies suggested some risk factors that could influence progress and survival in MSA, including the age at onset and initial clinical symptoms.[10,11] The distribution of the degeneration (neuronal loss/astrogliosis) and GCIs are thought to be system-related,[12] but duration and severity of the disease can possibly affect not only the distribution/density but also the immunohistochemical profile and regional preference of GCIs.[13] The correlation between neurodegenration/GCI accumulation and disease duration was systematically analyzed with autopsy cases.[14] Also, direct proportion of the severity of pathological changes to the disease duration was suggested by examining the long- and short-survival cases of MSAs.[15–18] However, the relationship between the disease

Correspondence: Toru Iwaki, MD, PhD, Department of Neuropathology, Neurological Institute, Graduate School of Medical Sciences, Kyushu University, 3-1-1 Maidashi, Higashi-ku, Fukuoka 812-8582, Japan. Email: iwaki@np.med.kyushu-u.ac.jp

Received 24 November 2010; revised 17 February 2011 and accepted 20 March 2011; published online 26 May 2011.

duration and the profile of GCIs in the entire CNS have not been systematically studied thus far.

We describe herein an autopsied case of MSA with prolonged clinical course of 18 years. By examining this particular case, we assessed the extent of the neurodegeneration and GCIs in the entire brain of this MSA case with long survival.

CLINICAL SUMMARY

A 64-year-old woman noticed gait disturbance, and subsequently developed dysarthria and dysphagia. There was no significant family history. Due to progression of symptoms, she became bedridden at the age of 69. Thereafter for 12 years, she had been fed through a nasogastric tube, and breathing was assisted through a tracheostomy due to central respiratory failure and repeated respiratory infections.

Neurological examination at the age of 78 disclosed limb and trunk ataxia, extrapyramidal and pyramidal signs (bradykinesia and brisk deep tendon reflexes), pseudobulbar/bulbar palsies, vocal cords paralysis and incontinence. She had no dementia, but displayed affective incontinence. She had no episode of orthostatic hypotension. Also, at the age of 78, MRI revealed severe atrophy of the cerebellum and the brainstem with "hot-cross bun sign" in the pons (Fig. 1A,B). Supratentorially, putaminal atrophy and frontal lobe-predominant cortical atrophy

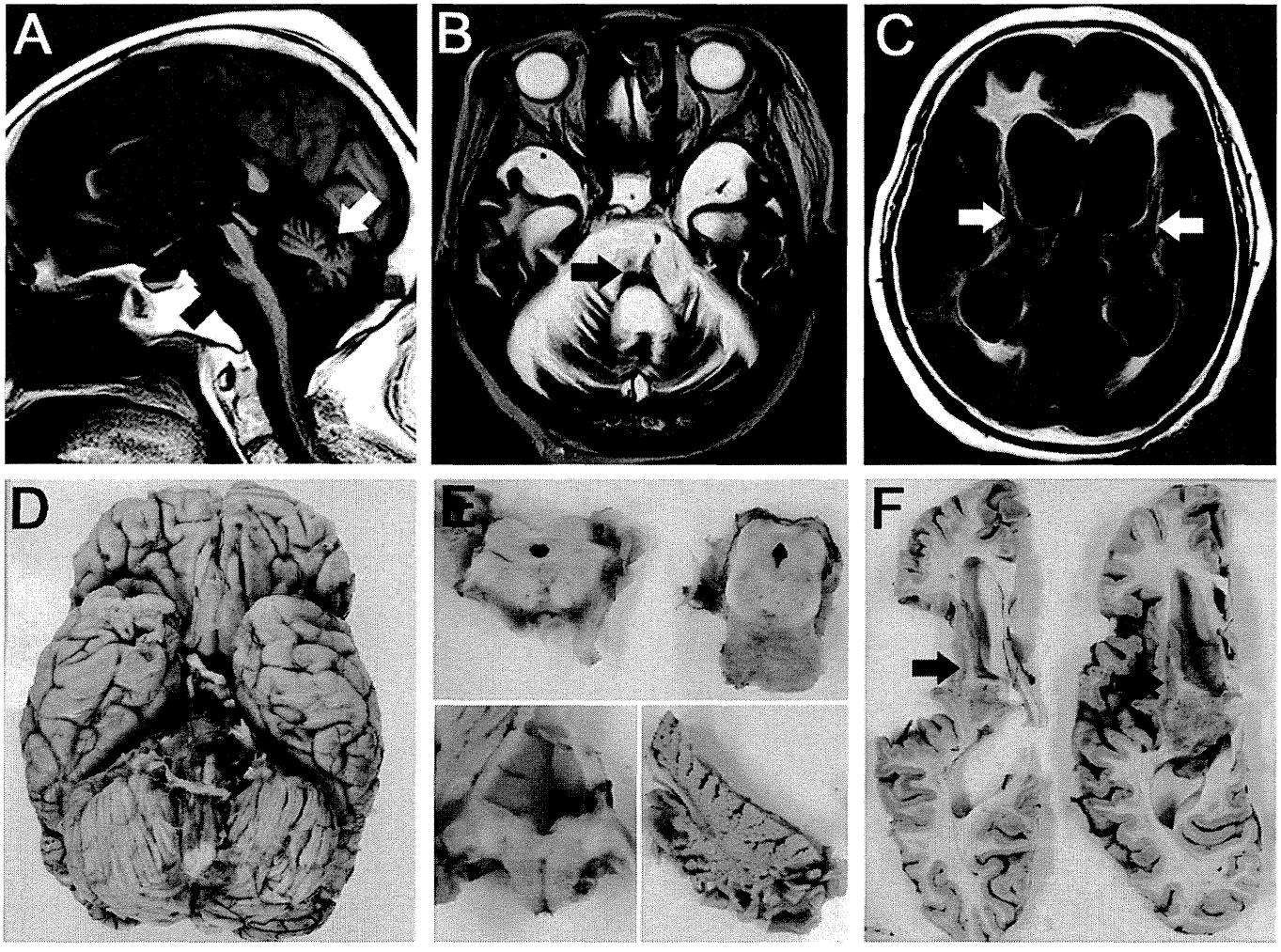

Fig. 1 Imaging studies (A–C) and macroscopic views (D–F) of the whole brain of the present case. (A) Severe atrophy of the cerebellum (white arrow) and the brainstem (black arrow) are prominent on T1-weighted MRI. (B) Signal change in the pons (hot-cross bun sign) is noted on T2-weighted MRI (arrow). (C) Fluid attenuated inversion recovery images also reveal cortical atrophy of the fronto-temporal lobe and putaminal atrophy with hypointensity (arrows). (D) From the basal view, there is severe atrophy in the cerebellum and the brainstem with brownish discoloration, and the bilateral frontal lobes are also atrophic. (E) The coronal sections of the brainstem show depigmentation of the substantia nigra, and severe atrophy of the pontine base (upper half), the inferior olive (lower left) and the cerebellum (lower right). (F) The horizontal sections of the cerebral hemisphere demonstrate putamen atrophy with brownish discoloration (arrows).

were also observed (Fig. 1C). According to the findings, she was diagnosed as MSA (OPCA).

Even after admission, her symptoms gradually worsened and she experienced repeated aspiration pneumonia and urinary tract infections. After a relapsing/remitting course of infections, she died of pneumonia at the age of 82 after 18 years from initial symptoms.

METHODS

Autopsy was conducted 3.5 h after death. Tissues were fixed in 10% formalin, and 5 μm-thick paraffin sections were cut. Sections were routinely stained with HE and KB stainings.

Immunohistochemical analysis was performed using the following antibodies: anti-phosphorylated α-synuclein (p-α-syn: Wako Pure Chemicals Industries, Ltd, Osaka, Japan, mouse monoclonal) used at a dilution of 1:1000; anti-ubiquitin (Ub: Dako A/S, Glostrup, Denmark, rabbit polyclonal) used at 1:1000; and anti-p62 (Enzo, Plymouth Meeting, PA, USA, rabbit polyclonal) used at 1:1000. All sections were deparaffinized in xylene and rehydrated in an ethanol gradient, and then were subjected to antigen retrieval by autoclaving in 0.01 mol/L citrate buffer, pH 7.0. Endogenous peroxidase activity was blocked with 0.3% H_2O_2/methanol. The sections were then incubated with primary antibody at 4°C overnight. After rinsing, the sections were subjected to the streptavidin-biotin complex method (for p62), the enhanced indirect immunoperoxidase method using Envision™ (DakoCytomation, Glostrup, Denmark) (for p-α-syn) or peroxidase-labeled goat anti-rabbit IgG (PI1000; Vector, Burlington, ONT, Canada) (for Ub). Immunoreactivity was detected using 3, 3′-diaminobenzidine (DAB), and sections were counterstained with hematoxylin. For double immunofluorescence study of GCIs, we used combinations of p-α-syn and p62 antibodies. FITC-conjugated (1:50; Southern Biotech, Birmingham, AL, USA) and Alexa Fluor 546 (1:200; Invitrogen, Carlsbad, CA, USA) secondary antibodies were used for detection. Sections were then examined under a confocal microscope (A1 Confocal Laser Microscope, Nikon Corporation, Tokyo, Japan).

The histological evaluation included semi-quantitative assessment of p-α-syn- or p62-postive GCIs in three randomly selected lesions from each region at ×200 power field: absent (0), very few (+), moderate (2+) and large numbers (3+).[19,20]

PATHOLOGICAL FINDINGS

On gross inspection, the brain weight was reduced to 900 g, and there was severe atrophy of the cerebellum and the brainstem (Fig. 1D). Sections of the brainstem showed decoloration of pigmented nuclei, including the substantia nigra, and atrophy with pontine base, the inferior olive and the cerebellar hemisphere (Fig. 1E). Sections of the cerebral hemisphere demonstrated that the putamen displayed severe atrophy with brownish discoloration (Fig. 1F), most prominent in its dorso-lateral zone of the caudal putamen.

Microscopic examination revealed severe neuronal loss and astrogliosis in the inferior olivary nucleus, pontine nuclei and basal ganglia, including the putamen (Fig. 2A). Marked loss of melanin-containing neurons was also observed in the substantia nigra and the locus ceruleus (data not shown). In the cerebellum, there was severe loss of both Purkinje cells and granular cells, as well as proliferation of Bergmann glia (data not shown). Notably, p-α-syn-positive GCIs and neuronal cytoplasmic inclusions (NCIs) were detected in the above-mentioned affected areas, but they were very few in number (Fig. 2B,C). However, it is interesting that p-α-syn-positive GCIs and NCIs were also present in the regions which usually contain a small number of GCIs, including tectum/tegmentum of the brainstem, pyramidal tracts, neocortices, limbic systems, thalamus and subthalamic nucleus (Fig. 2D–H), and the density of GCIs was much higher in these regions than in the archetypal lesions of MSA, such as olivo-ponto-cerebellar and striato-nigral systems (Table 1). In addition, the limbic system showed slightly higher density of GCIs/NCIs than in the neocortices.

α-syn and Ub are constituents of GCIs which are composed of fibrillary structures, and a staining profile of GCIs has been reported to be possibly related to both the duration of disease and regional preference.[13] The very long clinical course and characteristic distribution of GCIs in our MSA case prompted us to evaluate the Ub-distribution pattern in the entire brain. Ub and Ub-associated autophagy substrate p62[21] immunostainings confirmed that both antibodies could effectively detect GCIs at the same quantitative level, but the staining quality with p62 was clearer than that of Ub regarding background staining. Ub/p62+ typical-shaped GCIs were observed in the lesions where p-α-syn+ GCIs existed (Fig. 3A–D), and Ub/p62 and p-α-syn were colocalized in some GCIs (Fig. 3E). Distribution of Ub/p62 immunoreactivity was proportionate to that of p-α-syn+ GCIs, despite the very long duration of the present case (Table 1).

In addition to MSA-related systematic degenerations, hypoxic encephalopathy was evident both grossly and histologically, including pyramidal neuronal loss of the hippocampus, cerebellar infarction, cortical laminar necrosis and secondary myelin and axonal loss in the white matter (data not shown). Lots of p-α-syn+ GCIs were also distributed in the pale, deep white matter (data not shown), indicating the contribution of α-syncleinopathy as well as hypoxic effect to the lesions.

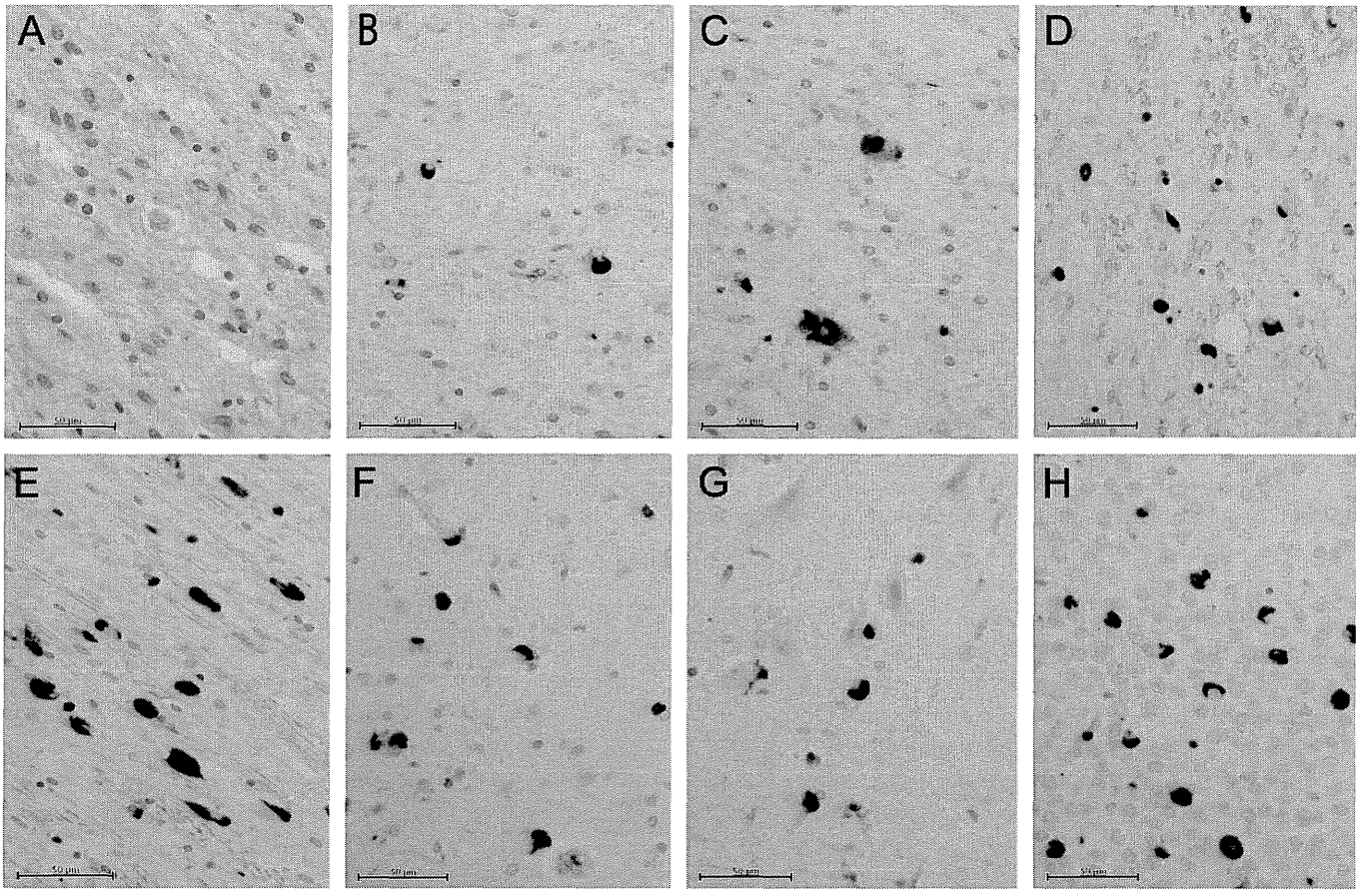

Fig. 2 Distributions of neurodegeneration and glial cytoplasmic inclusions (GCIs). (A) HE-stained specimen of the putamen shows severe neuronal loss, astrogliosis and rarefaction of the neuropil. (B,C) Immunohistochemistry reveals that a few p-α-syn+ small, ovoid/flame-shaped GCIs (B) and neuronal cytoplasmic inclusions (NCIs) (C) are noted in the degenerative putamen. (D,E) On the other hand, much larger numbers of p-α-syn+ GCIs are found in such regions as the tectum/tegmentum of the pons (D) and pyramidal tracts (internal capsules, E). (F–H) Also, p-α-syn+ GCIs unusually spread into the primary sensory cortex (postcentral gyrus, F), pyramidal cell layers (G) and granule cell layers (H) of the hippocampus. Note that the hippocampus, especially the granule cell layer, mainly exhibits NCIs rather than GCIs. Scale bars = 50 μm (A–H).

DISCUSSION

Multiple system atrophy is a rare, late-onset, and sporadic neurodegenerative disorder, the course of which is unfortunately merciless. Various factors have been proposed to predict survival in MSA, including gender, age of onset and clinical phenotype, although disagreements were also noted among these reports.[11,12,22–24] The median survival is about 8 years in MSA patients, but the spectrum is broad, reaching up to 15 years.[8]

From these standpoints, our MSA case showed an unusually long-term clinical course. Some reports suggested that earlier onset age and cerebellar symptoms as the initial manifestation could be better prognostic factors.[10] Our long-term survival case also presented with cerebellar symptoms as gait disturbance, but its onset age of 64 years was somewhat later-onset compared with the previous reports.[2,9] However, to determine the more accurate relationship between the clinical features and prognosis in MSA seems to be difficult because of the ambiguity in detecting early autonomic features preceding motor symptoms and signs.[10,23] Along with further population-based studies with the precise description of clinical symptoms, a different approach, including histopathological analyses, may be of assistance to unravel the difference between long-survival and short-survival cases of MSA.

The histological hallmark of MSA is the oligodendroglial inclusions, or GCIs. In addition, MSA is characterized by neuronal loss associated with astrogliosis. The degree of neuronal loss appears to be related to the duration of illness[25] and to the type of MSA.[26] Degenerative changes in our case were very severe, but mainly restricted to the systematically favorable site of MSA in spite of the long clinical course, excepting the hypoxic-damaged sites. In contrast, rather than the primary vulnerable areas, the density of GCIs and NCIs was higher in the primary

Table 1 Distribution of α-synuclein and ubiquitin pathology in GCIs of the entire brain region

Affected regions	Neocortical†								Limbic†							
	Frontal		Temporal		Parietal		Occipital		Cingulate gyrus		Amygdala		Hippocampus		Entorhinal	
0																
1+																
2+																
3+																

Affected regions	Basal ganglia										Cerebellum					
	Putamen		Globus pallidus		Caudate nucleus		Thalamus		Luysian body		Cortex		White matter		Dentate nucleus	
0																
1+																
2+																
3+																

Affected regions	Midbrain								Pons					
	Substantia nigra		Cerebral peduncle		Peri-aqueduct		III		Pontine nucleus		Locus ceruleus		Tectum/ tegmentum	
0														
1+														
2+														
3+														

Affected regions	Medulla oblonbata											
	Olive		Pyramidal tract		IX		X		XII		Cerebellar peduncle	
0												
1+												
2+												
3+												

† As for the limbic system, temporal/insular cortex, cingulate gyrus, amygdala and entorhinal cortex mainly displayed GCIs, and hippocampus, especially granule cell layers, exhibited NCIs rather than GCIs. Phosphorylated α-synuclein (p-α-syn) or p62-postive GCIs in three randomly-selected lesions from each region at ×200 power field are semi-quantitatively evaluated: absent (0), very few (+), moderate (2+), and large numbers (3+). Black: p-α-syn, gray: p62. III: nucleus nervi oculomotorii, IX: nucleus ambiguus, X: nucleus dorsalis nervi vagi, XII: nucleus nervi hypoglossi. The density of GCIs is much higher in the less-degenerated atypical regions than in the typical lesions of MSA, and the distribution of p62+ GCIs is proportionate to that of p-α-syn+ GCIs despite the very long clinical course. GCIs, glial cytoplasmic inclusions; NCIs, neuronal cytoplasmic inclusions.

sensory cortex (post-central gyrus and occipital lobe) and the limbic system, such as the cingulate gyrus, amygdala and hippocampus, in which GCI density is usually not so high, even in long-standing cases. It is considered that the occurrence of GCIs does not necessarily correlate with the degree of neuronal degeneration[12] nor the severity of astrocytosis.[27] In fact, the prevalence of GCIs in our case was inversely proportional to the severity of the neuronal loss and astrogliosis. Rather, it may reflect the duration of the disease, considering the fact that some patients with other neurodegenerative disorders who survive for a long time with support develop a widespread-type disease, showing extensive pathological involvement far beyond its original systems.[28] It is suggested that widespread α-synucleinopathy beyond OPC and SN systems might reflect the natural progression course of prolonged MSA cases. Alternatively, in our case, given that GCIs unusually spread in such lesions as primary sensory cortex and the limbic system, and the limbic system shows slightly higher density of GCIs/NCIs than neocortices do, the extensive lesion might be responsible for atypical symptoms such as affective disturbances.

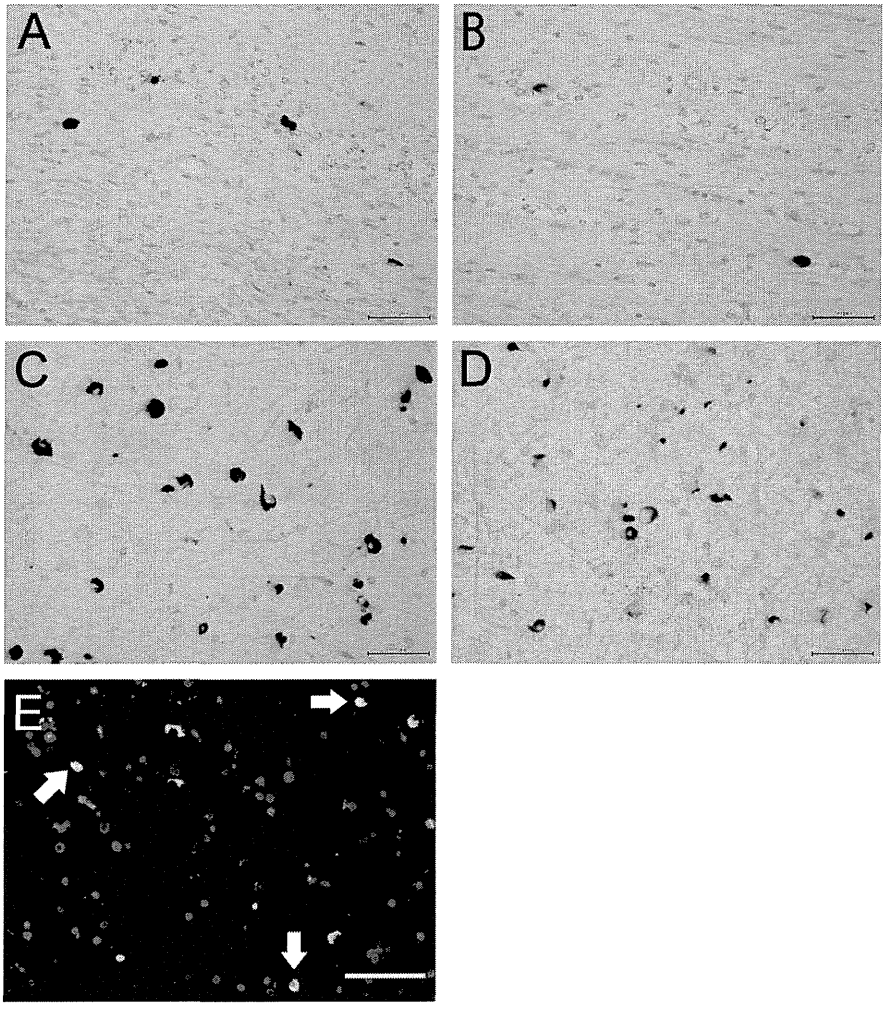

Fig. 3 Immunohistochemical profile of glial cytoplasmic inclusions (GCIs). (A–D) Immunohistochemically, Ub-related protein (p62)+ GCIs are present in the lesions (B: cerebellum, D: primary motor cortex) where p-α-syn+ GCIs are distributed (A: cerebellum, C: primary motor cortex). Interestingly, distribution of Ub/p62+ GCIs is parallel to p-α-syn+ GCIs in terms of the number/density. (E) Double immunofluorescence for p-α-syn (green) and p62 (red) on a section of primary motor cortex demonstrates crescent-shaped GCIs, and some GCIs are double-positive (arrows). Scale bars = 50 μm (A–E).

Glial cytoplasmic inclusions are composed of coated filaments with a diameter of 10–15 nm that are immunoreactive for Ub and α-syn. A certain staining profile of GCIs (α-syn–/Ub+) is possibly related to both the long duration of disease and to regional preference (a high prevalence of this profile in the motor cortex).[13] This is in contrast with cerebellar white matter where α-syn+/Ub+ GCIs are most prevalent.[13] As for our clinically prolonged case, distribution of Ub/p62 immunoreactivity was proportionately increased/decreased along with the density of p-α-syn GCIs. This is not necessarily contradictory to the finding that α-syn+/Ub– GCIs undertake a chronological change reciprocal to α-syn–/Ub+ GCIs, suggesting that α-syn immunoreactivity in GCIs is being replaced by Ub immunoreactivity during disease progression.[13] In the very long degenerative process seen in our case, α-syn–/Ub+ GCIs, which could follow α-syn+/Ub– GCIs after effacement of α-syn epitope and Ub accumulation,[13] might be further degraded and disappear due to Ub-related clearance processing. Further, in the midbrain, the density of GCIs is generally higher in the cerebral peduncle (white matter) than in the substantia nigra (gray matter) in the advanced stage of MSA. However, the substantia nigra in our case exhibited higher density of GCIs than the cerebral peduncle, which was severely atrophic owing to the very long disease course. This finding might be also relevant to the process of GCI formation and degradation. Further studies will be necessary for the elucidation of a process of GCI formation possibly linked to an aspect of degeneration, from the viewpoint of deposition of α-syn, Ub, p62 and their co-accumulation and disappearance.

Other than the MSA lesions, concurrent hypoxic encephalopathy was confirmed in our case probably due to the long clinical course with tracheostomy. The Gallyas-Braak staining and the immunoreactivity for α-syn and Ub are preserved even when the brain shows severe and diffuse softening due to respiratory arrest or respirator brain state, and the time lapse before the post mortem.[29] Actually, p-α-syn/p62+ GCIs can be detected irrespective of the hypoxic-damage state of the brain in our case. Thus, we can deduce from the findings that both hypoxia and

α-syncleinopathy could have contributed to the diffuse damage of the white matter in this MSA case, although many additional conditions such as cardiac arrest, hypotension and nutritional problems could be involved in long-course patients.

In summary, we report an autopsy case of MSA with prolonged clinical course, presenting extensive distribution of GCIs even in the less-degenerated areas and the involvement of the limbic system such as numerous NCIs in the dentate gyrus. This rare case suggests the possible contribution of the disease duration to the prevalence of GCIs.

ACKNOWLEDGMENTS

This study was supported in part by a Health and Labour Sciences Research Grant-in-Aid for Clinical Research from the National Hospital Organization (H21-NHO (Neuro-Muscular disorder)-03) and a Grant-in-Aid for Scientific Research (B) (No. 22300116) from Japan Society for the Promotion of Science (JSPS). The authors thank Ms. Sachiko Nagae (Department of Neuropathology, Kyushu University) for her excellent technical assistance.

REFERENCES

1. Gilman S, Wenning GK, Low PA *et al.* Second consensus statement on the diagnosis of multiple system atrophy. *Neurology* 2008; **71**: 670–676.
2. Lantos PL, Quinn N. Multiple system atrophy. In: Dickson DW, ed. *Neurodegeneration: The Molecular Pathology of Dementia and Movement Disorders.* Basel: ISN Neuropath Press, 2003; 203–214.
3. Papp MI, Kahn JE, Lantos PL. Glial cytoplasmic inclusions in the CNS of patients with multiple system atrophy (striatonigral degeneration, olivopontocerebellar atrophy and Shy-Drager syndrome). *J Neurol Sci* 1989; **94**: 79–100.
4. Nakazato Y, Yamazaki H, Hirato J, Ishida Y, Yamaguchi H. Oligodendroglial microtubular tangles in olivopontocerebellar atrophy. *J Neuropathol Exp Neurol* 1990; **49**: 521–530.
5. Wakabayashi K, Yoshimoto M, Tsuji S, Takahashi H. Alpha-synuclein immunoreactivity in glial cytoplasmic inclusions in multiple system atrophy. *Neurosci Lett* 1998; **249**: 180–182.
6. Mezey E, Dehejia A, Harta G, Papp MI, Polymeropoulos MH, Brownstein MJ. Alpha synuclein in neurodegenerative disorders: murderer or accomplice? *Nat Med* 1998; **4**: 755–757.
7. Gai WP, Power JH, Blumbergs PC, Blessing WW. Multiple-system atrophy: a new alpha-synuclein disease? *Lancet* 1998; **352**: 547–548.
8. Wenning GK, Stefanova N. Recent developments in multiple system atrophy. *J Neurol* 2009; **256**: 1791–1808.
9. Stefanova N, Bücke P, Duerr S, Wenning GK. Multiple system atrophy: an update. *Lancet Neurol* 2009; **8**: 1172–1178.
10. Ben-Shlomo Y, Wenning GK, Tison F, Quinn NP. Survival of patients with pathologically proven multiple system atrophy: a meta-analysis. *Neurology* 1997; **48**: 384–393.
11. Watanabe H, Saito Y, Terao S *et al.* Progression and prognosis in multiple system atrophy: an analysis of 230 Japanese patients. *Brain* 2002; **125**: 1070–1083.
12. Papp MI, Lantos PL. The distribution of oligodendroglial inclusions in multiple system atrophy and its relevance to clinical symptomatology. *Brain* 1994; **117**: 235–243.
13. Sakamoto M, Uchihara T, Nakamura A, Mizutani T, Mizusawa H. Progressive accumulation of ubiquitin and disappearance of alpha-synuclein epitope in multiple system atrophy-associated glial cytoplasmic inclusions: triple fluorescence study combined with Gallyas-Braak method. *Acta Neuropathol* 2005; **110**: 417–425.
14. Ozawa T, Paviour D, Quinn NP *et al.* The spectrum of pathological involvement of the striatonigral and olivopontocerebellar systems in multiple system atrophy: clinicopathological correlations. *Brain* 2004; **127**: 2657–2671.
15. Wakabayashi K, Ikeuchi T, Ishikawa A, Takahashi H. Multiple system atrophy with severe involvement of the motor cortical areas and cerebral white matter. *J Neurol Sci* 1998; **156**: 114–117.
16. Piao YS, Hayashi S, Hasegawa M *et al.* Co-localization of alpha-synuclein and phosphorylated tau in neuronal and glial cytoplasmic inclusions in a patient with multiple system atrophy of long duration. *Acta Neuropathol* 2001; **101**: 285–293.
17. Wakabayashi K, Mori F, Nishie M *et al.* An autopsy case of early ("minimal change") olivopontocerebellar atrophy (multiple system atrophy-cerebellar). *Acta Neuropathol* 2005; **110**: 185–190.
18. Fujishiro H, Ahn TB, Frigerio R *et al.* Glial cytoplasmic inclusions in neurologically normal elderly: prodromal multiple system atrophy? *Acta Neuropathol* 2008; **116**: 269–275.
19. Inoue M, Yagishita S, Ryo M, Hasegawa K, Amano N, Matsushita M. The distribution and dynamic density of oligodendroglial cytoplasmic inclusions (GCIs) in multiple system atrophy: a correlation between the density of GCIs and the degree of involvement of striatonigral and olivopontocerebellar systems. *Acta Neuropathol* 1997; **93**: 585–591.

20. Jellinger KA, Seppi K, Wenning GK. Grading of neuropathology in multiple system atrophy: proposal for a novel scale. *Mov Disord* 2005; **20**: S29–S36.
21. Pankiv S, Clausen TH, Lamark T *et al.* p62/SQSTM1 binds directly to Atg8/LC3 to facilitate degradation of ubiquitinated protein aggregates by autophagy. *J Biol Chem* 2007; **282**: 24131–24145.
22. Schrag A, Wenning GK, Quinn N, Ben-Shlomo Y. Survival in multiple system atrophy. *Mov Disord* 2008; **23**: 294–296.
23. Testa D, Filippini G, Farinotti M, Palazzini E, Caraceni T. Survival in multiple system atrophy: a study of prognostic factors in 59 cases. *J Neurol* 1996; **243**: 401–404.
24. Saito Y, Matsuoka Y, Takahashi A, Ohno Y. Survival of patients with multiple system atrophy. *Intern Med* 1994; **33**: 321–325.
25. Kume A, Takahashi A, Hashizume Y, Asai J. A histometrical and comparative study on Purkinje cell loss and olivary nucleus cell loss in multiple system atrophy. *J Neurol Sci* 1991; **101**: 178–186.
26. Tsuchiya K, Watabiki S, Sano M *et al.* Distribution of cerebellar cortical lesions in multiple system atrophy: a topographic neuropathological study of three autopsy cases in Japan. *J Neurol Sci* 1998; **155**: 80–85.
27. Fujita T, Doi M, Ogata T, Kanazawa I, Mizusawa H. Cerebral cortical pathology of sporadic olivopontocerebellar atrophy. *J Neurol Sci* 1993; **116**: 41–46.
28. Mizutani T, Aki M, Shiozawa R *et al.* Development of ophthalmoplegia in amyotrophic lateral sclerosis during long-term use of respirators. *J Neurol Sci* 1990; **99**: 311–319.
29. Nakajima M, Kojima H, Takazawa Y *et al.* An autopsy report on multiple system atrophy diagnosed immunohistochemically despite severe ischaemic damage: a new approach for investigation of medical practice associated deaths in Japan. *J Clin Pathol* 2009; **62**: 1029–1033.

Neurochemistry International 62 (2013) 330–339

Contents lists available at SciVerse ScienceDirect

Neurochemistry International

journal homepage: www.elsevier.com/locate/nci

GDNF promotes neurite outgrowth and upregulates galectin-1 through the RET/PI3K signaling in cultured adult rat dorsal root ganglion neurons

Shizuka Takaku [a], Hiroko Yanagisawa [a], Kazuhiko Watabe [a], Hidenori Horie [b], Toshihiko Kadoya [c], Kunihiko Sakumi [d], Yusaku Nakabeppu [d], Françoise Poirier [e], Kazunori Sango [a,*]

[a] ALS/Neuropathy Project, Tokyo Metropolitan Institute of Medical Science, Setagaya-ku, Tokyo 156-8506, Japan
[b] TechnoMaster Co. Ltd., Yokohama 236-0038, Japan
[c] Department of Biotechnology, Maebashi Institute of Technology, Maebashi, Gunma 371-0816, Japan
[d] Division of Neurofunctional Genomics, Department of Immunobiology and Neuroscience, Medical Institute of Bioregulation, Kyushu University, Fukuoka 812-8582, Japan
[e] The Department of Developmental Biology, Institut Jacques Monod, UMR 7592 CNRS, Paris-Diderot University, Paris, France

ARTICLE INFO

Article history:
Received 20 August 2012
Received in revised form 28 December 2012
Accepted 8 January 2013
Available online 20 January 2013

Keywords:
Galectin-1
Galectin-3
GDNF
Neurite outgrowth
Cell culture
Adult rat

ABSTRACT

Galectin-1 (GAL-1), a member of a family of β-galactoside binding animal lectins, is predominantly expressed in isolectin B4 (IB4)-binding small non-peptidergic (glial cell line-derived neurotrophic factor (GDNF)-responsive) sensory neurons in the sections of adult rat dorsal root ganglia (DRG), but its functional role and the regulatory mechanisms of its expression in the peripheral nervous system remain unclear. In the present study, both recombinant nerve growth factor (NGF) and GDNF (50 ng/ml) promoted neurite outgrowth from cultured adult rat DRG neurons, whereas GDNF, but not NGF, significantly increased the number of IB4-binding neurons and the relative protein expression of GAL-1 in the neuron-enriched culture of DRG. The GAL-1 expression in immortalized adult rat Schwann cells IFRS1 and DRG neuron-IFRS1 cocultures was unaltered by treatment with GDNF, which suggests that GDNF/GAL-1 signaling axis is more related to neurite outgrowth, rather than neuron-Schwann cell interactions. The GDNF-induced neurite outgrowth and GAL-1 upregulation were attenuated by anti-GDNF family receptor (RET) antibody and phosphatidyl inositol-3′-phosphate-kinase (PI3K) inhibitor LY294002, suggesting that the neurite-outgrowth promoting activity of GDNF may be attributable, at least partially, to the upregulation of GAL-1 through RET-PI3K pathway. On the contrary, no significant differences were observed between GAL-1 knockout and wild-type mice in DRG neurite outgrowth in the presence or absence of GDNF. Considerable immunohistochemical colocalization of GAL-3 with GAL-1 in DRG sections and GDNF-induced upregulation of GAL-3 in cultured DRG neurons imply the functional redundancy between these galectins.

1. Introduction

Galectin-1 (GAL-1), the first protein identified in a family of β-galactoside binding animal lectins, is involved in a wide variety of biological functions (Camby et al., 2006). It has been suggested that GAL-1 plays a role in the development and regeneration of the nervous system (Puche et al., 1996; Sakaguchi et al., 2010; Sango et al., 2012a) and the pathogenesis of neurological disorders, such as amyotrophic lateral sclerosis (ALS) (Kato et al., 2005), Parkinson's disease (Zhang et al., 2007), gliomas (Le Mercier et al., 2010), brain ischemia (Kurushima et al., 2005; Ishibashi et al., 2007), and immune-mediated peripheral neuropathies (Peng, 2012). GAL-1 is highly expressed in peripheral nervous tissues of adult rodents, with immunoreactivity localized to cell bodies of sensory and motoneurons, axons and Schwann cells. Facial nerve injury and interneuronal injection with glial cell line-derived neurotrophic factor (GDNF) enhanced GAL-1 mRNA in facial motoneurons (Akazawa et al., 2004; McGraw et al., 2004), but little is known about the mechanisms of how the expression of GAL-1 in mature sensory neurons is regulated. Predominant expression of GAL-1 mRNA/protein in subpopulations of small diameter dorsal root ganglion (DRG) neurons (Regan et al., 1986; Hynes et al., 1990; Imbe et al., 2003; Sango et al., 2004; McGraw et al., 2005a) suggests that this molecule plays a role in transmission of nociceptive and thermoceptive information (McGraw et al., 2005b). Adult DRG neurons can be divided into three principal subgroups by their soma size and characteristic markers; large neurons (immunoreactive for 200 kDa neurofilaments (RT-97 and N52)), small peptidergic neurons (immunoreactive for calcitonin gene-related peptide (CGRP) and high-affinity nerve growth factor (NGF) receptor

* Corresponding author. Address: ALS/Neuropathy Project (Laboratory of Peripheral Nerve Pathophysiology), Tokyo Metropolitan Institute of Medical Science, 2-1-6 Kamikitazawa, Setagaya-ku, Tokyo 156-8506, Japan. Tel.: +81 3 6834 2359; fax: +81 3 5316 3150.
E-mail address: sango-kz@igakuken.or.jp (K. Sango).

0197-0186/$ - see front matter © 2013 Elsevier Ltd. All rights reserved.
http://dx.doi.org/10.1016/j.neuint.2013.01.008

(trkA)), and small non-peptidergic neurons (immunoreactive for GDNF family receptor components (RET, GFRα1/2) and binding to isolectin B4 (IB4)) (Molliver et al., 1997; McMahon and Bennett, 2000). Imbe et al. (2003) performed immunohistochemistry and *in situ* hybridization using two pairs of consecutive DRG sections, and observed that almost all GAL-1 intensely labeled neurons displayed c-RET mRNA, but not CGRP mRNA. This finding agrees with our recent study employing double immunofluorescent staining (Sango et al., 2012a); almost all GAL-1 intensely labeled neurons were IB4-binding neurons and distinguished from CGRP and N-52 intensely labeled neurons. Since NGF and GDNF are likely to exert their major effects on small peptidergic (NGF-responsive) and non-peptidergic (GDNF-responsive) neurons, respectively, these findings led us to speculate that GDNF can modulate synthesis and/or distribution of GAL-1. In another study (McGraw et al., 2005a), however, GAL-1 immunoreactive neurons overlapped with both IB4-binding and CGRP-immunoreactive neurons in DRG sections. Following peripheral axotomy, GAL-1 expression was downregulated in small DRG neurons but was upregulated in large neurons (Imbe et al., 2003; McGraw et al., 2005a). These findings imply that retrogradely transported NGF and/or GDNF play a role in the dominant expression of GAL-1 in small DRG neurons.

Neuron-enriched primary culture of DRG cells from nearly 120 ganglia from 3 adult rats enables us to get sufficient amount of proteins for Western blot analysis and investigate the regulatory mechanisms and/or functional properties of neurotrophic factors such as NGF, GDNF, and ciliary neurotrophic factor (CNTF) (Sango et al., 2007, 2008). Our preliminary study employing this culture system revealed that GAL-1 expression was upregulated by exogenously applied GDNF, but not NGF (Sango et al., 2012a). The present study is aimed at elucidating the precise mechanisms for GDNF-induced GAL-1 upregulation, especially in association with the neurite outgrowth-promoting activity and the signaling pathways of GDNF.

2. Materials and methods

2.1. Animals

Three-month-old female Wistar rats were purchased from Japan Clea (Shizuoka, Japan). Three-month-old male and female GAL-1 knockout mice were gifted from Kyushu University (Kajitani et al., 2009). All experiments were conducted in accordance with the Guideline for the Care and Use of Animals (Tokyo Metropolitan Institute of Medical Science, 2011).

2.2. Cultures

Dissociated cell culture of adult rodent DRG neurons was performed as previously described (Sango et al., 2007). Briefly, DRG from the cervical to the lumbar level were dissected from each animal and dissociated with collagenase (Worthington Biochemicals, Freehold, NJ, USA) and trypsin (Sigma, St. Louis, MO, USA). These ganglia were subjected to density gradient centrifugation (5 min, 200g) with 30% Percoll (GE Healthcare Bio-Sciences Corp., Piscataway, NJ, USA) to eliminate the myelin sheath. This procedure resulted in a yield of more than 5×10^4 neurons along with a smaller number of non-neuronal cells such as Schwann cells, satellite cells and fibroblasts. The cells were rinsed once in serum-containing medium [Ham's F12 (Invitrogen Corp., Carlsbad, CA, USA) with 10% fetal bovine serum (FBS; Invitrogen)], once in serum-free medium [Ham's F12 with B27 supplement (Invitrogen)], and were suspended in serum-free medium and seeded on poly-L-lysine (PL, Sigma, 10 μg/ml)-coated wells of 8-well chamber slides (Nalge Nunc International, Naperville, IL, USA). The density of neurons was adjusted to approximately $2 \times 10^3/cm^2$ in each well.

Spontaneously immortalized Schwann cells established from adult Fischer rat, IFRS1 (Sango et al., 2011), were seeded onto 10 cm dishes at a density of $1–2 \times 10^4/cm^2$ and maintained in Dulbecco's Modified Eagles medium (DMEM, Sigma) supplemented with 5% FBS, 20 ng/ml heregulin-β (Upstate Biotech, Lake Placid, NY, USA) and 5 μM forskolin (Sigma). Coculture of IFRS1 with adult rat DRG neurons was conducted as described previously with slight modifications (Sango et al., 2011). Briefly, DRG neurons seeded on type I collagen (rat tail, Becton Dickinson, Bedford, MA, USA)-coated 6-well plates (Corning Inc., Corning, NY, USA) were maintained in serum-free medium for 7 days. Then, IFRS1 cells suspended in DMEM with 5% FBS were added to DRG neurons, adjusting the cell density ratio of neurons to IFRS1 cells to approximately 1:10. The coculture was maintained in serum-free medium supplemented with 50 μg/ml ascorbic acid in the presence or absence of 50 ng/ml recombinant rat GDNF (R&D Systems, Inc., Minneapolis, MN, USA).

2.3. Assays for neurite outgrowth

The following growth factors and inhibitors were used for the neurite outgrowth assays and Western blot analysis:

(1) recombinant rat β-NGF (R&D Systems);
(2) recombinant rat GDNF;
(3) recombinant mouse Neurturin (NRTN, R&D Systems);
(4) recombinant mouse Artemin (ARTN, R&D Systems);
(5) rabbit anti-RET polyclonal antibody [H-300] (Santa Cruz Biotech. Inc., Santa Cruz, CA, USA) (Plaza-Menacho et al., 2007);
(6) phosphatidyl inositol-3′-phosphate-kinase (PI3K) inhibitor LY294002 (Cell Signaling Technology Inc., Danvers, MA, USA); and
(7) mitogen-activated protein kinase (MAPK) kinase (MEK) inhibitor U0126 (Calbiochem; EMD Chemicals, Inc., San Diego, CA, USA).

At 16 h after seeding, cells were cultured in serum-free medium in the presence or absence of the growth factors (50 ng/ml) for up to 24 h. Our previous study showed that NGF and GDNF at the concentrations of 5, 50, and 500 ng/ml promoted neurite outgrowth, with the highest activity at 50 ng/ml (Sango et al., 2008). Based on those findings, we compared the bioactivity of each trophic molecule at 50 ng/ml in this study. Cells were then fixed with 100% methanol at −20 °C for 10 min, and incubated overnight at 4 °C with the mouse anti-βIII tubulin monoclonal antibody (1:1000; Sigma) (Vent et al., 2005). After rinsing with PBS, the cells were incubated for 1 h at 37 °C with peroxidase-conjugated anti-mouse IgG antibody (1:100; MBL Corp., Ltd., Nagoya, Japan). The immunoreaction was visualized under a light microscope using 0.01% diaminobenzidine tetrahydrochloride (DAB, Wako Co., Tokyo, Japan) and 0.01% hydrogen peroxide in 50 mM Tris buffer (pH7.4) at 37 °C for 15 min. We counted the number of neurite-bearing cells, defined as neurons having neurites with lengths that were longer than the cell body diameter (Sango et al., 2008). The ratios (%) of neurite-bearing cells were expressed relative to the total number of counted neurons (approximately 200) in each well. Neurite length was measured from digital images of the stained neurites using an image analyzing system (MetaMorph® System, Molecular Devices, Inc., Sunnyvale, CA, USA) (Tarsa and Goda, 2002). The length of the neurites (in micrometers) was expressed as the average value calculated from measurements of at least three different culture wells (30 neurites in each well) of each experimental group.

The detailed control experiments (Western blotting, pre-absorption tests, etc.) for the antibody against RET were described in the above articles and the Santa Cruz homepage [http://www.scbt.com/datasheet-13104-ret-h-300-antibody.html], which also indicate that this antibody is available for the functional assays, such as inactivation of RET.

Mouse laminin (LN: Becton Dickinson, 10 μg/ml), recombinant mouse GAL-1 and GAL-3 (R&D Systems, 0.1 μg/ml, 1 μg/ml and 10 μg/ml) were used as coating substrata. After removal of PL and following air-drying for 1 h, the PL-coated wells were further treated with each substratum for 1 h at room temperature.

2.4. Immunohistochemistry

The rats were anesthetized using isofluorane (Abott Japan, Tokyo, Japan), and perfused through the left cardiac ventricle with 100 mM PBS followed by acid-alcohol (95% ethanol and 5% acetic acid) or Bouin's solution without acetic acid (a mixture of 3 volumes of saturated picric acid solution to 1 volume of formalin). DRG dissected from the rats were processed for paraffin embedding and sectioned into 5-mm-thick slices. Deparaffined sections were incubated overnight at 4 °C with a mixture of the following antibodies and lectins that were diluted with 20 mM PBS containing 0.4% Block Ace (DS Pharma Biomedical Co., Osaka, Japan):

(1) mouse anti-GAL-3 monoclonal antibody (1:500; Abcam) (Byrnes et al., 2006) and rabbit anti-GAL-1 polyclonal antibody (1:1000; a gift from Kirin Pharma Co., Ltd., Takasaki, Japan) (Horie et al., 1999);
(2) mouse anti-GAL-3 monoclonal antibody and rabbit anti-neurofilament 200 monoclonal antibody (NF200, 1:1000, Sigma); and
(3) mouse anti-GAL-3 monoclonal antibody and Alexa Fluor 488-conjugated isolectin B4 (IB4, 1:1000; Invitrogen).

After rinsing with PBS, the sections incubated with anti-GAL-3 and anti-GAL-1 or anti-NF200 antibodies were then incubated in a mixture of Alexa Fluor 594 anti-mouse IgG and Alexa Fluor 488 anti-rabbit IgG antibodies (1:200, Invitrogen) for 1 h at 37 °C. The sections incubated with anti-GAL-3 antibody and IB4 were incubated with Alexa Fluor 594 anti-mouse IgG antibody. Immunohistochemical controls in which the primary antibodies were omitted resulted in lack of positive staining on each section (data not shown).

2.5. Immunocytochemistry

DRG neurons and IFRS1 cells were fixed with 4% paraformaldehyde for 10 min at 4 °C and then treated with 0.1% Triton X-100 in phosphate-buffered saline (PBS) for 5 min at room temperature. The cells were incubated overnight at 4 °C with a mixture of rabbit anti-GAL-1 polyclonal antibody and Alexa Fluor 594-conjugated isolectin B4 (IB4, 1:1000; Invitrogen). (Wu and Pan, 2004). After rinsing with PBS, the cells were incubated for 1 h at 37 °C with Alexa Fluor 488 anti-rabbit IgG antibody (1:200). Immunocytochemical controls in which the primary antibodies were omitted resulted in lack of positive staining on each culture sample (data not shown).

2.6. Image presentation

Cell culture samples processed for immunostaining were observed and recorded using a Zeiss Axiophoto microscope (Carl Zeiss Co., Ltd., Germany) equipped with a cooled CCD camera (Zeiss AxioCam) and Zeiss Axiovision software. When we manipulated the digital images using PhotoShop CS2 (Adobe Systems, Mountain View, CA, USA), adjustments for brightness and contrast were applied to the whole image, and did not enhance or eliminate any specific features present in the original images. When making merged images, we used same contrast levels (Rossner and Yamada, 2004).

2.7. Western blot analysis

The neuron-enriched DRG culture (>5 × 10^3/cm^2 at seeding) and the confluent culture of IFRS1 (>1 × 10^4/cm^2 at seeding) were prepared for Western blot analysis as previously described (Sango et al., 2008). SDS–PAGE was performed using 10% polyacrylamide gel. After electrophoresis, the proteins were transferred onto a nitrocellulose membrane (Bio-Rad, Hercules, CA, USA) with an electroblotter (Nihon Eido Co., Ltd., Tokyo, Japan). The membrane was incubated in a blotting solution (10 mM Tris, pH 7.4, 150 mM NaCl, 5% skimmed milk, 2% bovine serum albumin, and 0.1% Tween 20) for 2 h at room temperature, and then overnight at 4 °C with rabbit anti-GAL-1 polyclonal antibody (1:1000) or mouse anti-β-actin monoclonal antibody (Sigma, 1:1000) (North et al., 1993). After rinsing with PBS, the membrane was incubated in a solution of HRP-conjugated anti-rabbit or anti-mouse IgG (1:2000, MBL) for 2 h. After rinsing, immunocomplexes on the membrane were visualized with ECL plus a Western blotting detection kit (GE Healthcare Bio-Sciences). The signal intensity was quantified with Ez-Capture II chemiluminescence imaging system (Atto Corp, Tokyo, Japan), and the relative intensity of GAL-1 was expressed as the intensity of GAL-1/intensity of β-actin (Sango et al., 2012b).

2.8. Statistical analysis

All data are expressed as means ± SD. Parametric comparisons between experimental groups were performed by one-way analysis of variance (ANOVA). When ANOVA showed a significant difference between groups ($P < 0.05$), Tukey–Kramer test was used to identify which group differences accounted for the significant P value (Sango et al., 2008).

3. Results

3.1. Recombinant GDNF enhances neurite outgrowth, IB4 binding and protein expression of GAL-1 in cultured DRG cells

To prevent cell detachment and/or death at the initial stage in culture, DRG neurons were briefly incubated in the serum-containing medium prior to seeding (Sango et al., 2011). They were then maintained in serum-free conditions to avoid the effects of known and unknown factors contained in serum on neurite outgrowth and protein expression. The representative micrographs of immunostained DRG neurons, as well as the ratios of neurite-bearing cells (%) and average neurite length (μm), in each experimental group after 2 days in culture are shown in Fig. 1. In agreement with previous studies (Leclere et al., 1998; Paveliv et al., 2004; Sango et al., 2008, 2012a), treatment with each trophic molecule significantly increased the ratios of neurite-bearing cells, whereas NRTN and ARTN showed less potent activities than NGF and GDNF on the average neurite length. Immnocytochemical analysis showed intense immounoreactivity for GAL-1 in almost all cultured DRG neurons in each group. Treatment with GDNF failed to further increase the GAL-1 immunoreactivity, but significantly increased the number of IB4-binding neurons (Fig. 2A and B).

Western blot analysis with neuron-enriched DRG culture revealed the signals of GAL-1 and β-actin corresponding to molecular weight of 14.5 kDa and 42 kDa, respectively (North et al., 1993; Sango et al., 2004), with more intense signals for GAL-1 in the GDNF-treated group than those in the control and NGF-treated groups. The quantitative studies indicate that GDNF significantly

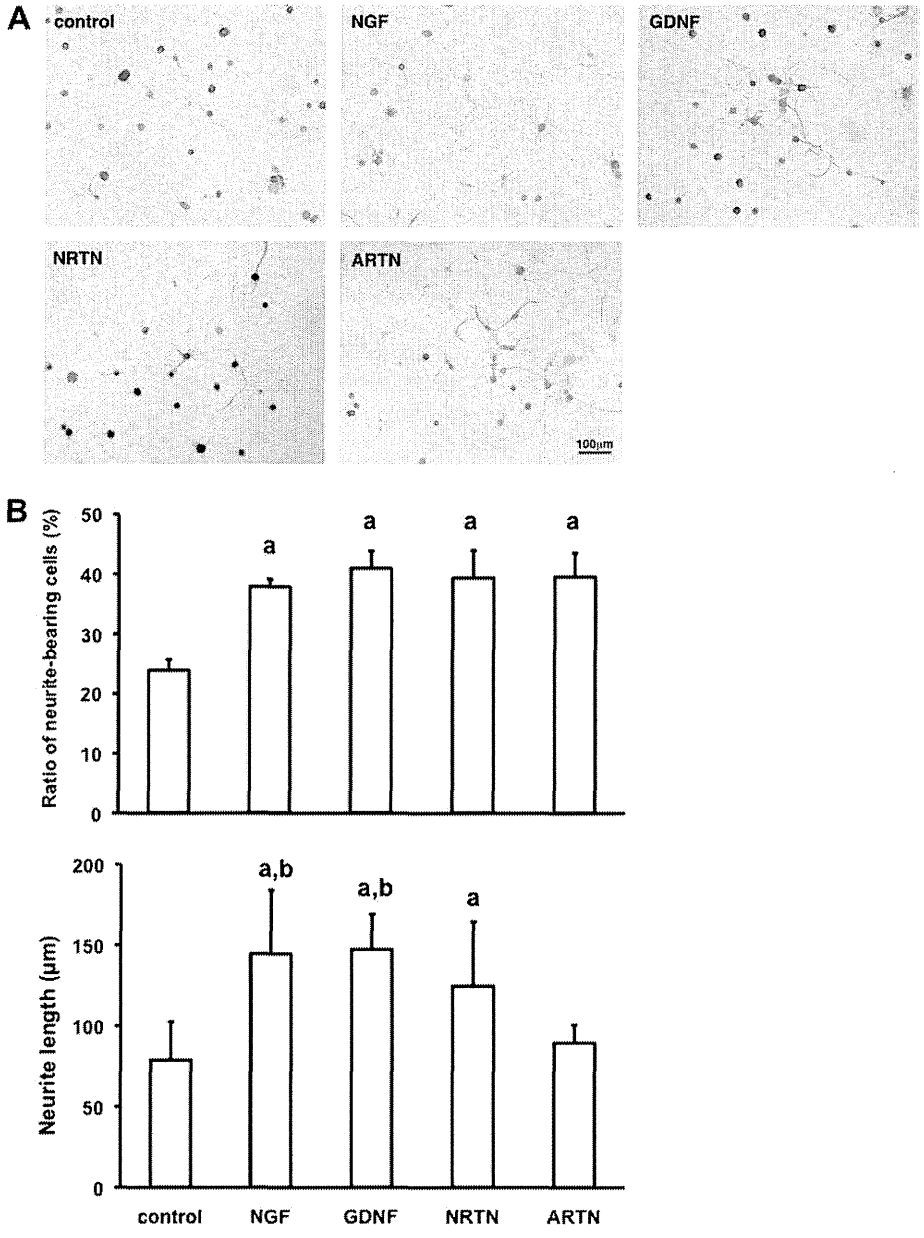

Fig. 1. NGF and GDNF family of ligands (GDNF, NRTN, ARTN) enhance neurite outgrowth from cultured adult rat DRG neurons. (A) Representative photomicrographs of DRG neurons immunostained with anti-βIII tubulin. (B) Bar charts of the ratios (%) of neurite-bearing cells and average neurite length (μm) after 2 days in culture. Values represent the means and SD of 6–9 experiments with 3 animals. a: $P < 0.05$ as compared with control, b: $P < 0.05$ as compared with ARTN.

($P < 0.05$) upregulates protein expression of GAL-1 in cultured DRG cells, whereas NGF has no effects (Fig. 2C left). In other experiments, NRTN and ARTN showed bioactivity of GAL-1 upregulation comparable to GDNF, but the differences in the values between the NRTN- or ARTN-treated group and the control group were not statistically significant (Fig. 2C right). The approximate molecular weight of recombinant rat GDNF (15 kDa) is similar to that of rat β-NGF (13 kDa), mouse NRTN (12 kDa) and mouse ARTN (12 kDa), and it seems reasonable to compare the biological effects of these molecules at the same concentration (50 ng/ml).

3.2. GDNF fails to upregulate GAL-1 expression in the immortalized Schwann cells IFRS1

IFRS1 cells showed distinct Schwann cell phenotypes, such as spindle-shaped morphology under phase-contrast microscopy, expression of Schwann cell markers (*e.g.* S100, p75 low affinity neurotrophin receptor), and fundamental ability to myelinate neurites in coculture with DRG neurons (Sango et al., 2011) and differentiated PC12 cells (Sango et al., 2012b). We observed the intense immunoreactivity for GAL-1 in the cell bodies and processes of IFRS1 cells (Fig. 3A). These expression patterns are similar to those in primary cultured Schwann cells (Paratcha et al., 2003; Sango et al., 2004). In contrast to the significant effects on DRG cells, neither NGF nor GDNF induced apparent morphological changes or GAL-1 immunoreactivity of IFRS1 cells (not shown). The quantitative Western blot analysis resulted in no significant differences in GAL-1 expression among the 3 groups (Fig. 3B). GDNF has been shown to promote myelination in cocultured DRG neurons and IFRS1 cells (Sango et al., 2011), but it failed to upregulate GAL-1 expression in the same coculture system (Fig. 3C and D).

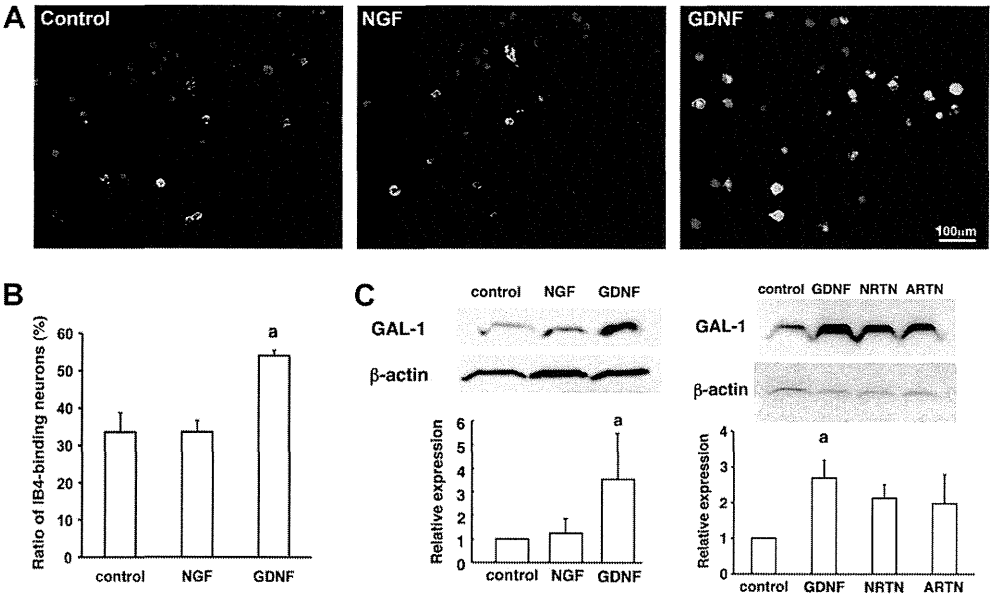

Fig. 2. GDNF, but not NGF, increases the ratios of IB4-binding neurons and upregulates the expression of GAL-1 in DRG cells after 2 days in culture. (A) DRG neurons in control, NGF-treated, and GDNF-treated groups were immunostained for GAL-1 (red) and IB4 (green). (B) Effects of recombinant NGF and GDNF (50 ng/ml) on the ratios (%) of IB4-binding neurons. Values represent the means and SD of 4 experiments with 2 animals. a: $P < 0.05$ as compared with control. (C) (Upper) Representative Western blots; the expression bands of GAL-1 and β-actin are identified as the level a molecular size of around 14 kDa and 42 kDa, respectively. (Lower) The protein expression of GAL-1 in NGF- and GDNF-treated cells (Light) and GDNF-, NRTN-, and ARTN-treated cells (Right) relative to that in untreated cells (control). Values represent the means and SD of 3–5 experiments with 30 animals. a: $P < 0.05$ as compared with control.

3.3. Involvement of RET and PI3K signaling pathway in GDNF-induced neurite outgrowth and upregulation of GAL-1 expression

Since neurite outgrowth and GAL-1 expression were enhanced by NRTN and ARTN, as well as GDNF, we speculated that common signaling pathways through the activation of RET receptor are involved in the bioactivity of these molecules in cultured DRG neurons. The neurite outgrowth assays (Fig. 4A) and Western blot analysis (Fig. 4B) revealed that GDNF-induced neurite outgrowth and upregulation of the GAL-1 expression were significantly suppressed by co-treatment with the anti-RET antibody (2 μg/ml). To further elucidate the downstream signaling pathways, we used a pharmacological inhibitor of PI3K, LY294002 (25 μM) and that of the MEK, U0126 (25 μM). The neurite outgrowth assays (Fig. 4A) and Western blot analysis (Fig. 4C) revealed that the promoting activities of GDNF on neurite outgrowth and GAL-1 expression were totally attenuated by co-treatment with LY294002, but not with U01296.

3.4. Findings from GAL-1 knockout mice imply functional redundancies between GAL-1 and GAL-3

In stark contrast to the findings described above, we observed no significant differences in the neurite outgrowth activity between the GAL-1 knockout and wild type mice in the presence or absence of GDNF (Fig. 5). These findings led us to speculate functional redundancies between GAL-1 and other molecules, especially other galectin family members (Wang et al., 2006; Tsai et al., 2011). We observed that GAL-3 is abundantly expressed in small GAL-1-immunoreactive and IB4-binding DRG neurons (Fig. 6A). Moreover, Western blot analysis showed that GDNF upregulated GAL-3, as well as GAL-1, in neuron-enriched culture of DRG (Fig. 6B). Taking these findings into consideration, GAL-3 may be another target molecule for the GDNF signaling in DRG neurons.

3.5. Bioactivities of recombinant GAL-1 and GAL-3 on neurite outgrowth

Recombinant GAL-1 and GAL-3 at the concentration of 0.1 μg/ml, 1 μg/ml, or 10 μg/ml was applied to culture dishes precoated with poly-L-lysine. LN is recognized as a potent inducer of neurite outgrowth, and we used it as a positive control in the assay (Sango et al., 2003). GAL-3 at 0.1 μg/ml and 1 μg/ml significantly increased the ratios of neurite-bearing cells after 2 days in culture. In contrast, GAL-1 at any concentration failed to show neurite-outgrowth promoting activity (Fig. 6C). We observed no significant effects of either galectins on the average neurite length (data not shown).

4. Discussion

In the present study, treatment with recombinant NGF and GDNF (50 ng/ml) significantly promoted neurite outgrowth from adult rat DRG neurons after 2 days in culture. These findings agree with those in previous studies (Gavazzi et al., 1999; Sango et al., 2008), where both molecules mainly acted on small diameter neurons. In contrast to the results of neurite outgrowth assays, Western blot analysis revealed that GDNF, but not NGF, significantly upregulated GAL-1 expression. This finding suggests that GAL-1 is one of the downstream target molecules of GDNF in cultured DRG cells. NGF has been shown to induce expression of GAL-3, another member of the galectin family, in cultured neonatal mouse DRG neurons (Pesheva et al., 2000) and differentiating PC12 cells (Kuklinski et al., 2003). In contrast to those studies, we observed no significant effects of NGF on the expression of GAL-1 and GAL-3 in mature DRG neurons. Considering that both GAL-1 and GAL-3 are predominantly expressed in small DRG neurons of rats from embryonic to mature stages (Regan et al., 1986), the differential responses to NGF between neonatal and mature DRG neurons appear to be attributable, at least partially, to postnatal phenotypic switching of small IB4-binding neurons from NGF to GDNF dependence (Molliver et al., 1997). It is also noteworthy that mice lacking GAL-1 showed reduced proportion of IB4-binding DRG neurons